2021-11-01

Characterizing Hydration of the Ocean Crust Using Shortwave Infrared Microimaging Spectroscopy of ICDP Oman Drilling Project Cores

Crotteau, MA

10.1029/2021jb022676
Journal of Geophysical Research: Solid Earth
American Geophysical Union (AGU)

Characterizing Hydration of the Ocean Crust Using Shortwave Infrared Microimaging Spectroscopy of ICDP Oman Drilling Project Cores

Molly A. Crotteau[1*], Rebecca N. Greenberger[1], Bethany L. Ehlmann[1], George R. Rossman[1], Michelle Harris[2], Peter B. Kelemen[3], Damon A. H. Teagle[4], and the Oman Drilling Project Phase 1 Science Party

[1]Division of Geological and Planetary Sciences, California Institute of Technology, 1200 E. California Blvd., Pasadena, CA, 91125, USA

[2]School of Geography, Earth and Environmental Sciences, Plymouth University, Plymouth, PL4 8AA, UK

[3]Department of Earth & Environmental Sciences, Columbia University, Lamont–Doherty Earth Observatory, Palisades, NY 10964, USA

[4]School of Ocean and Earth Science, National Oceanography Centre Southampton, University of Southampton, European Way, Southampton, SO14 3ZH, UK

Corresponding author: Molly Crotteau (mollycrotteau@ucsb.edu)

*Now at Department of Earth Science, University of California Santa Barbara

Key Points:

- An infrared spectral index using the area of OH/H_2O absorptions at ~1400 nm spatially maps and quantifies H_2O in rocks with high accuracy.
- The hydration ranges from 0 to 18 wt.% H_2O with mean and medians for sheeted dike and gabbroic cores ranging from 1.5 to 3.2 wt.% H_2O.
- Deeper gabbroic oceanic crust is more hydrated due to relative prevalence of zeolite minerals and fault zones that facilitate hydration.

eywords: Oman Drilling Project, ocean crust, ophiolite, crustal hydration, water quantification, infrared imaging spectroscopy

Abstract

Although ocean crust covers over 60% of Earth's surface, the processes that form, cool, and alter the ocean crust are not completely understood. We utilize shortwave infrared micro-imaging spectroscopy of ~1.2 km of rock cored by the International Continental Scientific Drilling Program's Oman Drilling Project to quantify hydration of basaltic dikes and gabbros from the Samail ophiolite as a function of depth, mineralogy and deformation. We develop a regression (R^2=0.66) between area of the ~1350-1650nm OH/H_2O absorption and measurements of loss on ignition of samples and apply this relationship to generate quantitative ~250 μm/pixel hydration maps for all cores. The lowest mean hydration is observed in the most pervasively altered dike-gabbro boundary (GT3A, H_2O_{mean}=2.1±1.6 wt%), consistent with the low H_2O content of the dominant alteration minerals, amphibole and epidote. The highest H_2O content occurs in deeper foliated and layered gabbros (GT2A, H_2O_{mean}=3.2±3.0 wt%) and layered gabbros (GT1A, H_2O_{mean}=2.8±3.1 wt%). The greater prevalence with depth of zeolite alteration as opposed to lower wt% H_2O amphibole at shallow stratigraphic depths, as well as the occurrence of zones of intensive hydration associated with fault zones (H_2O_{mean}=5.7±4.0 wt%) lead to greater hydration of the lower ocean crust. This new approach provides an objective quantification of hydration in these cores, enabling an improved understanding of quantities and characteristics of ocean crust hydration. It highlights the importance of specific phases and faulting in controlling hydration, which has implications for ocean crust cooling, rheological properties, and the role of alteration in global biogeochemical cycling.

Plain Language Summary

Ocean crust makes up much of Earth's crust. When it forms and cools, it reacts with seawater and other fluids to trap water in rock. The goal of this study was to determine how much water is stored within the ocean crust. We measured rock cores drilled from an ophiolite, a place where ocean crust has been thrust onto land. We used an infrared imaging spectrometer, commonly used on spacecraft to survey other planets, to measure reflected light as a function of wavelength to make maps of the amount of water in the core to determine what controls where the water is held in different minerals. We developed a method to determine the amount of water in the rocks using wavelength-dependent patterns in absorptions in reflected light. Most of the ocean crust contains 1.5 – 3.2% water by weight. Surprisingly, the mid ocean crust sampled by our cores has the least amount of water, whereas the lower segments have more water. This is due to the presence in the cores of specific minerals called zeolites that form at low temperatures and the high extent of hydration in the rocks surrounding deep fault zones.

1 Introduction

Although the ocean crust covers over 60% of the Earth, it is not completely understood how the basaltic and gabbroic ocean crust forms, cools, and is chemically altered by seawater. The location and intensity of chemical exchanges between seawater and the ocean crust impacts global biogeochemical cycles and influences mechanisms for the accretion of new ocean crust. Consequently, it is important to improve our understanding of the ways in which the ocean crust formed and has been modified by fluid-rock interactions (e.g., Coggon et al., 2016; Harris et al., 2017; Alt and Teagle. 1999; Kelemen et al., 1997). Moreover, subduction of altered oceanic crust – together with altered mantle peridotite and H_2O-bearing sediments – is the main input of molecularly bound H_2O into the Earth's upper mantle, where it drives volcanic arc magmatism, contributes to formation and evolution of continental crust, and reduces the viscosity of the convecting mantle (e.g., Hacker, 2008; Campbell and Taylor, 1983; Blacic, 1972; Chopra and Paterson, 1984). Thus, quantifying the H_2O content of oceanic crust is essential to understand the planetary water cycle.

It has been challenging to observe and measure relevant parameters because deep drilling of intact, in situ the ocean crust has proved very challenging (Michibayashi et al., 2019). Consequently, study of the magmatic accretion and hydrothermal exchange processes in the ocean crust has required the investigation of ophiolites: ancient sections of ocean crust and upper mantle formed at some style of ocean spreading center, now preserved on-land. Recently, the International Continental Scientific Drilling Program (ICDP) Oman Drilling Project (OmanDP) has drilled cores from ocean crust exposed in the mountains of Oman (Kelemen et al., 2020; Kelemen et al., 2013). These cores provide selected continuous sections of oceanic crust representative of specific intervals of the mid to lower ocean crust preserved in the Samail ophiolite. On-land diamond coring returned cores with near-100% recovery avoiding the drill sampling bias that commonly affects igneous rock sampling by scientific ocean drilling (e.g. Tominaga et al., 2009).

OmanDP recovered ~3.2 km of rock from nine boreholes within the Samail ophiolite in Oman, which formed at a fast-spreading, submarine spreading center (e.g., Tilton et al., 1981; Rioux et al., 2012) and is the largest and best exposed section of oceanic lithosphere and upper mantle preserved on-land (Glennie et al., 1973; Searle and Cox, 1999) (Fig. 1). Although trace element and geochronological data indicate that the Samail spreading center formed above a subduction zone, the crust formed via crystallization of primitive magmas very similar to parental mid-ocean ridge basalts (e.g., Pearce et al., 1981; MacLeod et al., 2013; Rioux et al., 2016). Although weathering and obduction may have further altered the ophiolite, the signatures of seafloor alteration remain. Key OmanDP objectives include better understanding of the formation of ocean lithosphere at mid-ocean ridges, seafloor hydrothermal alteration, ocean-crust-mantle mass transfer, and weathering processes (Kelemen et al., 2013; Kelemen et al., 2020).

Processes in the mantle, the hydrosphere, the atmosphere, and the biosphere drive crustal hydration and alteration (e.g., Shuai and Yang, 2017). Water stored within minerals is the dominant reservoir of water on Earth, and the quantification of water in minerals and rocks illuminates the processes of hydration and alteration in the crust and, through subduction, impact the water budgets of the mantle (e.g., Bell and Rossman, 1992). Previous studies have measured bulk water contents of the ocean crust sampled by scientific ocean drilling ranging from 1 to 8 wt% H_2O in the upper oceanic crust and from 0.1 to 0.5 wt% H_2O in the lower gabbros (Agrinier et al., 1995a, 1995b; Alt et al., 1996; Godard et al., 2009; Kawahata et al., 1987; Kleine et al., 2020; Kusakabe

et al., 1989; Jarrad, 2003; Shilobreeva et al., 2011; Coggan et al., 2016). However, core recovery is low for the lavas and dikes of the upper ocean crust (Alt et al., 1996), and cumulate gabbros have not been reached in intact ocean crust (Teagle et al., 2012). As a result of low recovery, more altered and fragile materials are underrepresented in the cores (Tominaga et al., 2009), leading to probable underestimates of the abundance of H_2O and other seawater-derived tracers in the ocean crust. In this study, access to core with near-complete recovery enables a more complete quantification of water content of the ocean crust, providing crustal hydration data for the wide range of materials, depths, and tectonic settings.

Spatially resolved infrared spectroscopy is non-contact, requires no sample preparation, and provides a method to map hydration non-destructively and contiguously at small spatial scales to address both the overall water content of the ocean crust and factors driving its heterogeneity. The entire OmanDP drill core was scanned with an imaging spectrometer at a spatial resolution of 250-260 μm/pixel (Greenberger et al., 2021), and here we develop methods that utilize this dataset to quantify and map the water content of the crust. Water in rocks occurs as both H_2O and hydroxyl OH groups, usually bonded with a metal in a mineral structure. In this study, we use "water" to refer to OH/H_2O collectively. Water has a number of absorptions in shortwave infrared, including the fundamental stretch of metal-OH (~2700-2800 nm), the fundamental stretch of H_2O (2760-3000 nm), and the fundamental bend of H_2O (6000-6200 nm) (e.g., Bishop et al., 1994, 2002). Absorptions from 2700 to 3000 nm are commonly used in transmission spectroscopy to quantify water in minerals (Rossman, 2006). In single crystal mineral samples, infrared spectroscopy quantitatively determines the amount of water present within a mineral (Potter and Rossman, 1979; Bell et al., 1995; Libowitsky and Rossman, 1996; Libowitsky and Rossman, 1997; Rossman, 2006; Shuai and Yang, 2017). In geologic samples, the 2700 nm OH and H_2O fundamental absorptions, which occur when a vibrational state is excited from $\upsilon = 0$ to $\upsilon = 1$, have been shown to correlate directly with hydration in particulate minerals and mineral mixtures, irrespective of composition (Milliken and Mustard, 2005). However, for this study, we do not have spectral data at wavelengths longer than 2600 nm. Instead, we develop and apply methods based on additional absorptions of OH/H_2O that do occur in our spectral range: combination absorptions that occur when two or more fundamental absorption modes combine, and overtone absorptions that occur near integer multiples of the fundamental absorption modes. For minerals in the OmanDP core, these include metal-OH overtones (1380-1560 nm), H_2O combination tones (1410-1460 nm), and H_2O combination tones (1910-1970 nm) (Bishop et al., 1994, 2002; White et al., 2017). Prior studies with particulate geologic materials have shown the 1900-nm H_2O combination band increases with increasing weight percent H_2O with mineral-specific dependencies (Milliken and Mustard, 2005).

We first develop and then apply infrared methods to quantify and map hydration at sub-millimeter scale over ~1.2-km of ocean crustal core from OmanDP Holes GT1A, GT2A, and GT3A. These three boreholes sample 400 m-deep sections of layered gabbros (GT1A), foliated and layered gabbros (GT2A), and the transition from sheeted dikes to gabbros (GT3A) (Fig. 1; Kelemen et al., 2020). Using a combination of traditional geochemical measurements of loss on ignition (LOI) and imaging spectroscopy data, this study quantifies the spatially resolved hydration of the ocean crust and its variation, using a novel infrared spectral index. By examining the spatial patterns of hydration and alteration as a function of depth, mineralogy, and fault occurrence, we gain insight into the ways in which ocean crust cooled and was altered by hydrothermal fluids.

2 Methods

2.1 Determination of loss on ignition

Published loss on ignition (LOI) data, collected in the laboratories of the D/V *Chikyu* by the OmanDP science team during the ChikyuOman2017 core description campaign (Kelemen et al., 2020), were used to develop correlations between spectral indices and H_2O content of rocks. Methods for determination of loss on ignition of OmanDP samples from Holes GT3A, GT2A, and GT1A are described in detail in Kelemen et al., (2020) and summarized here. After acquisition, the core was split into an archive half and a working half. Destructive analyses were performed on the working half following detailed core description. Representative whole-rock geochemical samples with adjacent oriented thin sections were cut with a diamond rock saw as either 5-cm or 8-cm long quarter-round sections. Core surface altered rinds were removed. The sections were then cut into thin slices, and saw marks were removed with 220 μm sandpaper. Samples from GT1A and GT2A were then ultrasonicated in ethyl alcohol for 10 minutes and in deionized water 3 times for 10 minutes to clean them. Samples from borehole GT3A were ultrasonicated in deionized water 3 times for 10 minutes. Samples were dried for 6 h at 105°C, crushed to <5 mm, and then crushed to <2 mm in the Spex SamplePrep 3630 X-Press. To prepare fine powders for analysis, samples were further ground using a Fritsch Pulverisette 5 planetary mill with agate grinding bowls and agate balls.

Samples were weighed using the OHTI (Ocean High Technology, Institute, Inc., Tokyo, Japan) balance system into a ceramic crucible. 5 g were used for samples from boreholes GT1A and GT2A, and 2-3 g were used for samples from borehole GT3A. The balance was calibrated at the beginning of the ChikyuOman2017 core description phase, and calibration was verified every 12 h. Samples were then dried at 105°C for 2 hr to remove adsorbed water, cooled to room temperature in a desiccator, and reweighed. The powder was then ignited at 1000°C for 3 hr. The powder was cooled, placed in a glass desiccator, and reweighed to determine LOI. We correct those measurements for CO_2 and SO_2 also determined aboard (Table S1) by subtracting the measured CO_2 and volatile S contents from LOI. We then use the corrected LOI as the basis of comparison with water quantification from imaging spectroscopy data.

It has also been noted that the oxidation of Fe in samples during heating may increase the residual sample weight thereby reducing the measured LOI (Kelemen et al., 2020; Lechler and Desilets, 1987). If all Fe had been present as Fe^{2+} and it was all oxidized, then the H_2O from LOI would be on average 0.8 wt% greater. However, given that iron oxides and epidote containing Fe^{3+} are present in the core, it would be incorrect to assume that all the iron was initially present as Fe^{2+}. Because the Fe^{2+} to Fe^{3+} ratio is unknown as is the extent of any oxidation during the procedure, we choose not to correct for Fe oxidation. Different choices in method of H_2O calculation from LOI only lead to H_2O changes in all holes at the ≤1 wt% level, affecting each hole in a similar manner (Text S1, Table S1).

2.2 Imaging spectroscopy

Imaging spectroscopy, also known as hyperspectral imaging, is a technique which enables the user to combine both spatial and spectral data to determine information about a material and the abundance and/or state of an absorbing species (Goetz et al., 1985; Clark et al., 2003). Absorptions

present in spectra correspond to chemical bonds and can be used to determine the mineralogy and the amount of water and hydroxide in minerals and rocks (e.g., Burns, 1993; Clark et al., 1990; Hunt, 1977; Stolper, 1982; Hammer et al., 1996; Jamtveit et al., 2001; Bell et al., 2003; Johnson and Rossman, 2003; Bell et al., 2004; Milliken and Mustard, 2005; Asimow et al., 2006; Milliken and Mustard, 2007; Schuttlefield et al., 2007). Our method of reflectance imaging spectroscopy of the core is non-destructive, enabling acquisition of whole core hydration at sub-millimeter scale with spatial context preserved and requiring no sample preparation. In contrast, although transmittance spectroscopy has demonstrated accuracy for hydration determinations, it requires destructive sampling of the core and consequently can only be applied to small regions of samples.

Methods for the imaging spectroscopy data acquisition and mineral mapping are described in detail in Kelemen et al. (2020), a companion paper (Greenberger et al., 2021), and summarized here. Imaging spectroscopy measurements were obtained on the archive halves of the OmanDP cores in August-September 2017 with the Caltech Ehlmann laboratory's pushbroom imaging spectrometer, which acquires line-by-line a cross-core spatial row of pixels, measuring reflected light; each pixel has a corresponding spectrum. This instrument has both a visible-near infrared (VNIR; 0.4 – 1.0 μm) and a shortwave infrared (SWIR; 1.0 – 2.6 μm) sensor. For this study, the data from the SWIR sensor was used because the relevant OH/H_2O absorption features are in that wavelength range. The SWIR data were acquired at 6 nm spectral resolution, 6 nm spectral sampling, and 250-260 μm/pixel spatial resolution for the HQ core and 260 μm/pixel for the NQ core with exposure times of 4.5 – 5.4 ms. After every 4 – 6 images, the spectrometer was calibrated with measurements of dark current and a Spectralon reference target.

The data were stored as spectral image cubes, and regions of interest (ROIs) were defined and outlined in ENVI software using known depths of the geochemical samples used for LOI and thin section images. Using the automated methods of Greenberger et al., (2021), pixels in the images that were not the rock core (i.e. pixels containing the plastic core liner or Styrofoam) were identified and excluded from further analysis. We also used methods described in Greenberger et al. (2021) to combine analyses of all core sections from each borehole to create a continuous length of core with depths assigned. For calculation of mean, median, and standard deviation statistics, pixels 65-214 in the horizontal or x-direction were used for the larger diameter HQ-size core sampled at 250 μm/pixel and pixels 65-220 for NQ-size core sampled at 260 μm/pixel. There are 4% fewer pixels vertically in the coarser resolution of NQ core, so we compensate with 4% more pixels in the horizontal direction. This sub-sampling ensures that approximately the same number of pixels per meter are included in calculation of statistics and removes sample size biases from downhole changes in core diameter and spatial resolution. For downhole statistics aggregated at 10 cm or 1 m spacing, we use all pixels that contain the core within each interval. Data from miscellaneous core, designated "M" (Kelemen et al., 2020) where portions of holes were re-drilled, are excluded from our downhole analyses.

2.3 Calculation of integrated absorption area

While simple absorption band intensities for a sample can vary depending on the instrument's polarizer and spectroscopic resolution, absorption band areas do not vary significantly as a result of changes in polarization and resolution (Rossman, 2006). The relationship between integrated absorbance and the amount of water in a mineral has been successfully determined for single crystals but has yet to be extensively studied in bulk rocks (Shuai and Yang, 2017).

The integrated band areas of the H_2O combination absorptions (1900 nm) and the OH overtone and H_2O combination absorptions (1350 nm – 1650 nm) were both initially calculated in this study (Fig. 2). In order to obtain the integrated areas of these two bands, we first smoothed the imaging spectroscopy data with the boxcar averaging SMOOTH function in IDL with a width of 3 in all dimensions (spatial x and y and spectral). The average reflectance value is then plotted at the central wavelength and pixel value for the sample. This treatment was particularly important for the low H_2O, dark samples, where the H_2O and OH absorptions are small in magnitude and a positive or negative spike from noise has a large effect on the subsequent continuum removal and band area quantification (Fig. 2i). By smoothing the spectrum, the magnitude of noise is decreased, which provides a more accurate measure of the depth of the H_2O combination and OH overtone absorptions. Although some of the sharpness of hydroxyl absorptions is lost, perhaps yielding a slight underestimation, the overall effect is to remove spurious data points. The effects of smoothing are shown in Figure 2 for a high hydration, moderate hydration, and low hydration pixel.

A continuum removal was then performed on spectral subsets of the smoothed spectrum utilizing the CONTINUUM_REMOVE_DOIT function in IDL. This function uses a convex hull fit to remove the continuum from the spectrum in every pixel in the hyperspectral images of the cores. To calculate H_2O concentrations pixel-by-pixel in the core, we first derived integrated band areas for each pixel using the continuum removed spectra and a rectangle approximation method. With this method, a rectangle width is defined as halfway between the prior bandpass and the center bandpass to halfway between the center bandpass and the next bandpass. The height of the rectangle is defined as one minus the reflectance measurement of each spectral band, i.e., the area between the continuum (1.0) and the continuum removed spectrum. The area of the rectangle is then the width of the rectangle multiplied by the height of the midpoint, and the total area of the absorption is defined as the sum of the areas of all the rectangles defined across the range. The results of the rectangular approximation varied by <1% from the computationally slower five-point Newton-Cotes approximation using the INT_TABULATED function in IDL.

We continuum removed and calculated band area for the H_2O combination region from 1823 nm – 2100 nm (5485 – 4762 cm^{-1}) and the OH overtone and H_2O combination region from 1355 nm – 1654 nm (7380 – 6046 cm^{-1}). We evaluated four different means of calculating continuum-removed band areas: (1) the 1900-nm band area with units of wavenumber, (2) 1900-nm band area with units of wavelength, (3) the 1400-nm band area with units of wavenumber, and (4) the 1400-nm band area with units of wavelength.

Although raw data from the instrument were in units of wavelength, the motivation for the evaluation of the continuum removal in units of wavenumber is because it is a unit of energy. Absorption of light energy is directly related the type and quantity of minerals, and wavenumber is therefore commonly used for quantification of materials with spectroscopy (e.g., Libowitsky and Rossman, 1997; Rossman, 2006; Bell et al., 1995; Potter and Rossman, 1979; Shuai and Yang, 2017; Sunshine et al., 1990). Because the conversion between wavelength and wavenumber is not linear, band area calculations in units of wavelength and wavenumber result in slight differences in the distribution of values.

2.4 Mapping hydration with integrated area vs. hydration relationships

In order to determine the relationship between hydration and integrated band area of the four different calculated OH/H_2O band areas, we considered the LOI measurements obtained from whole rock samples in Holes GT1A, GT2A, and GT3A. ROIs were defined in the imaging spectroscopy data of the archive half of core that corresponded to the depths and core widths sampled in the working core. The mean integrated area of each sample was calculated by taking the mean of all integrated areas calculated for each pixel in the defined ROIs with each of the four different band area calculation methods (Table S2).

Linear regressions fit through (0, 0) were calculated for each of the four different band area calculations between integrated area and measured LOI (Fig. 3). We excluded data from two samples of uncommon rock types that had weak absorption features with low integrated areas but high measured H_2O values. The inclusion of these samples in the regression decreased the accuracy of our H_2O estimation for more common rock types composing the vast majority of the rock from these three boreholes. One sample excluded from the regression came from GT1A 41Z-2, 98.26 – 99.16 m. In the igneous core description logs, this site was defined as a disseminated oxide olivine mela gabbro, present only between 96.36 m – 101.23 m in Hole GT1A (1.2% of Hole GT1A and ~0.4% of all the core considered in this study) (Kelemen et al., 2020). The second excluded ROI was dunite (serpentinized) from GT1A 107Z-3, which only occurs in two depth intervals totaling 23 cm in Hole GT1A (~0.06% of Hole GT1A and ~0.02% of all core included in this study) (Kelemen et al., 2020). Both rock types are very dark, and prior work has shown that the depths of absorption features of OH and H_2O are affected by darkening agents such a magnetite, spinels, and sulfides (Milliken and Mustard, 2007). These rock types are rare in the OmanDP holes considered in this study and the great majority of the plutonic ocean crust. However, these rock types are present in some IODP sites and dunites and other highly serpentinized rocks are common around the crust-mantle boundary. For the quantification of hydration in cores where these rock types are abundant, different calibrations may need to be determined specifically for these very dark colored rocks.

For all four band area calculations, integrated band area increases with increasing hydration as measured by LOI in an approximately linear manner (Fig. 3). This relationship determines wt.% H_2O with average errors of 0.52 ± 0.49 wt.% (Table S3) and shows more scatter at <2-3 wt. % H_2O. The R^2 value between the integrated area and measured LOI is the highest (R^2 = 0.66) when using the continuum removed spectrum for the ~1400-nm absorption in wavenumber units ($BA_{1400,wavenum}$) with the equation

$$Calculated\ wt.\%\ H_2O = 0.0761 \times BA_{1400,wavenum} \quad (1)$$

To map hydration in the entire core, the area of the OH overtone absorption was calculated for each pixel utilizing the smoothed and continuum removed spectrum in wavenumbers for each pixel and Equation 1.

3 Results

The LOI measurements used in this paper yield H_2O contents of 0.058 – 9.75 wt%. For further discussion of the LOI results, see Kelemen et al. (2020).

3.1 Mapping core hydration

Hydration maps were calculated for all core sections using the equation derived in Section 2 (Figures S1-3). Examples of the hydration maps for core sections with LOI samples indicating high OH/H_2O, intermediate OH/H_2O, and low OH/H_2O are shown in Figure 4. Hydration maps of the core show a high degree of spatial coherency and detail. Transitions between high hydration and low hydration regions correspond to and commonly follow the boundaries of subtle color differences present in color images of core section that indicate different rock types or degrees of alteration. There is very little speckling in hydration maps that could indicate noise or discrepancies in band calculation. Instead, the hydration maps in fact reveal more structural complexity in veins and fractures than the standard color imagery. Mineralized fractures and veins present in the cores are commonly sites of higher hydration. Most veins and fractures are surrounded by halos of slightly more hydrated rock.

Downhole plots of calculated H_2O estimates with 1 meter and 10 centimeter averages for each borehole are shown in Figure 5. At a spatial resolution of 250-260 μm/pixel, hydration in these boreholes ranges from 0 to 20 wt% H_2O. Over 85% of the ocean crust has hydration values of less than 5 wt% H_2O. Qualitatively, all three holes have similar values for most intervals without systematic hydration change as a function of depth (Fig. 5). However, Holes GT2A and GT1A have substantially more high hydration excursions. The dike-gabbro transition Hole GT3A exhibits the lowest mean H_2O (2.1 ± 1.6 wt%), whereas intermediate depth Hole GT2A that samples mid-crustal foliated and layered gabbros, exhibits the highest mean H_2O (3.2 ± 3.0 wt%) (Table 1). The mean hydration of lower crustal Hole GT1A (2.8 ± 3.1 wt%) is between the means of Hole GT2A and Hole GT3A. However, in terms of median hydration, a different trend is observed. Across all three holes, the median H_2O is lower than the mean H_2O. This is likely due to zones containing very hydrated pixel band areas, such as pixels containing primarily zeolite, particularly thomsonite and laumontite, that drive up the mean H_2O significantly. Hole GT2A has the highest median H_2O (2.2 wt%), but Holes GT3A and GT1A have much lower medians (1.7 wt% and 1.5 wt%, respectively). In GT1A, many of the high hydration depth intervals are associated with faults (Fig. 5). Other high hydration intervals are caused by proximity to minor fault or damage zones (e.g., at 315 m and 360 m in Hole GT1A, Fig. 5) or increased abundances of high-H_2O zeolite minerals (e.g., at 65 m in Hole GT1A, Fig. 5; see Greenberger et al., 2021 for mineral occurrence maps). The controls on H_2O in the ocean crust is an important question and a topic that we are continuing to explore. However, the purpose of this paper is to provide quantitative estimates of H_2O within the ocean crust and some initial discussion of the controls on its distribution. A thorough analysis of the causes of all high H_2O zones and their significance – as well as increases in concentration of key minerals – is beyond the scope of this paper, and a prime topic for future research.

In order to understand the calculated mean and median H_2O and the range of H_2O contents between holes GT3A, GT2A, and GT1A, we consider the variations in hydration values and generate histograms of H_2O content for each hole (Fig. 6). From Figure 6, it is evident that, while the much of the core from all boreholes has 0.5 – 2% H_2O, GT2A and GT1A have longer tails towards higher H_2O values. ~37% of Hole GT2A by area has H_2O concentrations >3 wt%. In contrast, only ~30% of Hole GT1A and ~19% of Hole GT3A by area have H_2O concentrations >3 wt%. Approximately 60 wt% of Holes GT1A and GT3A are <2 wt% H_2O by area whereas only ~47% of Hole GT2A by area is <2 wt% H_2O. Thus, it is evident that Hole GT2A has more zones of elevated H_2O, likely composed of high H_2O content minerals, relative to Holes GT1A and GT3A.

3.2 Mineral carriers of hydration

Both the visual core logging (Kelemen et al., 2020) and determination of spatial occurrences of key minerals (Greenberger et al., 2021) found that Hole GT3A exhibits the most pervasive alteration as measured by its lowest occurrence of primary minerals and highest occurrence of secondary minerals, yet we find the lowest levels of hydration in Hole GT3A. Thus, there are factors beyond simply alteration driving the hydration of the ocean crust, likely the type of secondary minerals formed. Comparing mean hydration of each 1-m length of core and the percentage of pixels within that meter that contained the mineral of interest from Greenberger et al., (2021) provides a means of understanding the carrier phases of hydration in the ocean crust. While overall hydration increases with alteration of primary igneous minerals, the specific phases of the alteration mineralogy appear to be one of the most important drivers of changes in degree of bulk hydration with depth (Figure 7). Natural pyroxenes commonly host ~50-100 ppm OH (Skogby et al., 1990), but to first order, in its unaltered form, pyroxene ($(Ca,Mg,Fe)Si_2O_6$) contains very little water. As expected, with increasing frequency of pyroxene mapped in a given meter of core, the predicted H_2O decreases. This trend is observed in Figure 7a, indicating that the mineralogical and the hydration data are consistent with each other. Holes GT1A and GT2A, which have more unaltered pyroxene than Hole GT3A, clearly exhibit the expected correlation of hydration increase and pyroxene decrease, clearly indicating that alteration drives hydration.

The most commonly occurring alteration mineral is chlorite, and hydration is observed to increase monotonically with abundance of chlorite (Fig. 7b). The relationship is different for each hole, however, with a relatively modest increase in hydration for each wt% chlorite for GT3A and greater increases for GT1A and GT2A. This may be due to the overall abundance of chlorite and the role of accessory phases that are in mineral assemblages with chlorite. Prehnite and zeolite are more common spatially in Hole GT1A and Hole GT2A compared to Hole GT3A (Greenberger et al., 2021). Zeolite minerals contain on the order of ~15 wt% H_2O. Regions of the core which have the highest prevalence of epidote tend to converge to hydration values of ~3% (Fig. 7e). Areas of very high hydration have relatively low epidote abundance of less than 20%, indicating that the water contents in regions of high hydration in the ocean crust are dominated by water in zeolites. Higher abundances of zeolite and zeolite-prehnite assemblages in Hole GT2A and GT1A may be driving their higher mean hydration values, and the lower frequency of these minerals in Hole GT3A may explain its lower predicted H_2O values (Fig. 7c and 7d). (We note that limitations in the mapping of Greenberger et al., 2021, prohibit identification of zeolites in pixels with the 1.48 µm overtone of OH that is diagnostic of prehnite, resulting in likely underestimation of zeolite proportion.) Thus, although hydration increases with increased alteration, the specific minerals

formed as a result of alteration processes are important in affecting the overall amount of water sequestered at different depths of the crust.

3.3 Hydration and its correlation with structural features

Faults are observed throughout the boreholes (Kelemen et al., 2020). Although fault zones are common in Holes GT3A and GT2A, we use only the major fault zones in Hole GT1A in this study to understand the role of major fault zones in hydration, alteration, and cooling of the ocean crust because this hole was located to sample such horizons (Kelemen et al., 2020) and has surface correlation with a major fault zone (Zihlmann et al., 2018). Fault zones have previously been shown to be associated with intense hydrothermal alteration (Bruhn et al., 1994; Zihlmann et al., 2018) and have been proposed as important conduits for fluid circulation in and cooling of the lower oceanic crust (Coogan et al., 2006; Harris et al., 2017). Using the depths of major fault zones recorded by the OmanDP core description teams (Kelemen et al., 2020), we compare H_2O concentrations for rock within fault zones and outside of major fault zones in Hole GT1A (Table 2; Fig. 8) and find dramatic differences in hydration. Hydration is significantly higher in the major fault zones (mean H_2O = 5.7 wt%) compared to the regions outside of major fault zones (mean H_2O = 2.6 wt%) (Table 2). The median hydration of the fault zones is still high (4.7 wt%), indicating that the very high hydration pixels are common throughout the fault zones.

The high hydration within the fault zones of Hole GT1A correlates with the significant occurrences of alteration minerals, particularly amphibole and chlorite + prehnite + zeolite assemblages, detected by Greenberger et al., (2021). Additionally, the regions of Hole GT1A outside of major fault zones generally exhibit minimal alteration and low hydration, providing evidence that hydration and alteration of the lower ocean crust are driven by fault zones as conduits of hydrothermal fluid, highlighting the combined roles of physical fracturing and chemical alteration.

4 Discussion

4.1 Accuracy of spectral indices and sources of error

The infrared spectral index developed in this paper, band area of the 1400-1600 nm OH/H_2O absorptions calculated in wavenumber, displays a strong positive correlation with measured wt% H_2O. On average, the errors between the measured H_2O samples and the H_2O calculated by our model are of magnitude 0.52 ± 0.49 wt% H_2O (Table S3). The R^2 value for this regression (0.66) is only slightly lower than R^2 values determined in other studies that use reflectance data. With their controlled grain size particulate mixtures of bright, water-bearing samples, Milliken and Mustard (2005), found R^2 values ranging from 0.74 – 0.96 using methods including the mean optical path length, normalized optical path length, integrated band area, and effective single-particle absorption thickness for the OH fundamental absorption at ~2900 nm. Our more complex, dark, multi-mineralic rock samples unsurprisingly have lower R^2 values due to use of the weaker overtone and combination absorptions and variations in grain size, which can affect absorption. Nevertheless, the correlation between the area of the OH overtone absorption and the measured wt% H_2O still provides means for effective tracking of spatial variability non-destructively and comprehensively at very fine scale.

There are a few instances where we more significantly overestimate or underestimate H_2O. In the geochemical samples, ~5% of samples had low 1400-nm band areas (<20) but higher LOI H_2O measurements (>2 wt%) (Table S3). These 13 samples can be observed in Figure 3d. Our method therefore could result in the underestimation of the H_2O content in some regions of the core. The weaker than expected OH absorption features in these samples are likely due to textural and mineralogical effects, such as the presence of darkening agents, particularly serpentinized, opaque, or dark colored minerals, that affect the depths of absorption features (Milliken and Mustard, 2007).

One unavoidable source of error in the regression pertains to the way in which geochemical measurements were obtained. Samples for geochemical measurements including LOI were taken from the working half of the core, whereas the imaging spectroscopy data was obtained from the archive half (Kelemen et al., 2020). Although these two halves are close to mirror images of each other, they are not identical. In addition, geochemical measurements of LOI are three-dimensional measurements of a volume of rock crushed to powder that included material from below the surface of the split face of the working half. In contrast, imaging spectroscopy maps hydration for a two-dimensional measurement of the surface. The depth of penetration of light at the wavelengths of the imaging spectrometer is approximately tens to hundreds of micrometers (Hapke, 2012). Thus, the regression developed between integrated area of the 1.4-μm band and the measurement of LOI actually compares measurements of slightly different materials. If a vein is present in the interior of the rock cut for geochemical measurements but not in the archive half of the core or vice versa, the calculated H_2O from spectra would and should differ from the volume measured. A second related inherent error in our data is the fact that the precise location of the ROIs is difficult to constrain. Through the use of the core logging tables and images of thin sections (Kelemen et al., 2020), we worked to locate as precisely as possible exactly where the samples were taken. However, the exact regions we defined as ROIs in the imaging spectroscopy data may be slightly offset from their actual location and differ in exact size and shape.

Although two LOI samples were excluded from the regression, these samples represent rock types that are uncommon in the ocean crust considered in this study. Consequently, their exclusion does not introduce significant sampling bias. Our methods work well for the analysis of gabbros and basalts, which are predominant rock types in the ocean crust. Both highly altered and unaltered sections of the ocean crust are included in this analysis, enabling a more complete understanding of ocean crust hydration. Samples with low wt% H_2O determined via LOI measurements also almost always have low H_2O as determined via spectroscopy, with errors as described previously, and the technique works well with higher H_2O samples, with the exception of a couple uncommon rock types, different from the calibration set.

Overall, this study has shown the value of microimaging spectroscopy as a tool to use in conjunction with conventional LOI methods. While LOI measurements do provide wt% H_2O data with high precision, they are time-consuming and destructive. Microimaging spectroscopy can be used to take millions or billions of measurements quickly and non-destructively. Although less precise, the average error of spectroscopic H_2O calculations in comparison with traditional LOI measurements was ~0.5 wt.% H_2O. In addition, microimaging spectroscopy can be performed on any sample and does not require complete core recovery or unharmed core. Furthermore, there are no biases related to sampling strategy. For different rock types and other core samples, a similar workflow could be used to obtain a regression equation relating integrated area via imaging

spectroscopy to H_2O LOI measurements and then apply this equation to construct whole-core maps.

4.2 Hydration of the ocean crust

The Oman ophiolite records hydrothermal alteration and metamorphism, mostly absent overprinting by weathering or obduction (e.g. Kawahata et al., 2001; A'Shaikh et al., 2006, Pflumio et al., 1991). Overall, we find that the H_2O content of the ocean crust at 250-260 μm/pixel spatial resolution in the OmanDP core ranges between approximately 0 and 18 wt% H_2O, with the majority of the ocean crust containing 0.5 – 3 wt% H_2O. Hole GT2A (foliated and layered gabbros) is the most hydrated borehole in this study, with both the highest mean and median hydration values. Hole GT1A (layered gabbros) has a slightly lower mean H_2O than GT2A, but a much lower median H_2O (Table 1), suggesting that the majority of GT1A is low hydration, with a small volume of zones characterized by high hydration. Interestingly, despite being closest to the ocean floor, the uppermost Hole GT3A (dike-gabbro transition) has the lowest calculated mean and median H_2O. There are more very hydrated zones in GT1A compared to GT3A, driving the mean H_2O of GT1A higher than that of GT3A. The larger amount of high H_2O zones in GT1A is likely a result of the fact that Hole GT1A contains ~2 times as much high H_2O content zeolite as Hole GT3A, likely due to the presence of relatively more low temperature fluid circulation, (Greenberger et al., 2021) and has extensive mineralized fault zones (Kelemen et al., 2020).

Overall, our results differ somewhat from existing estimates of oceanic crust H_2O content. Our results fall in the range measured in the Troodos Massif gabbros, where H_2O values ranged between 0 – 7.5 wt% H_2O (Moores and Vine, 1971). More recently, Kleine et al., (2020) estimated H_2O in altered basalts from the on-land section of the Mid-Atlantic Ridge ranging from 0.5 – 9.1 wt%. Using δD values measured in previous work (Kawahata et al., 1987; Shilobreeva et al., 2011; Agrinier et al., 1995a, 1995b; Kusakabe et al., 1989; Coogon et al., 2016), H_2O has been estimated to be 1.6 ± 1.3 wt% in the volcanic ocean crust, 1.6 ± 0.6 wt% in the sheeted dikes, and 0.8 ± 0.1% in the gabbros (Kleine et al., 2020). Their average H_2O estimate in the sheeted dikes is similar to our study (2.1 wt% for GT3A). However, the mean values of 2.8 wt% for GT1A and 3.2 wt% for GT2A are indicative of higher values for oceanic gabbro H_2O than those previously calculated. This is likely a result of the fact that the core recovery in previous ocean drilling is biased toward mostly unaltered sections of the core, whereas our whole core mapping includes crustal H_2O estimates for both the altered and unaltered sections of the ocean crust since onland diamond drilling provides ~ 100% recovery of cored sections, both altered and unaltered. Previous IODP studies of ocean crust have generally suffered from lower core recovery. For example, Hole 1309 on the Atlantis Massif recovered an average of 75% of the core (Blackman et al., 2006). Similarly, Site U1473 on the Southwest Indian Ridge achieved an average of 59% core recovery (Macleod et al., 2017). Site 894 at Hess Deep (Leg 147) only achieved a core recovery of 27.5% in the upper mantle rocks (Früh-Green et al., 1996). Typical samples in previous studies focused on a single rock type and tended to exclude veins and other major structural features (e.g., Shilobreeva et al., 2011). In contrast, we include veins, fault zones, and damage zones in our calculations, and these features tend to have higher H_2O values as a result of their higher H_2O mineralogy and alteration, leading to higher hydration values. Thus, the range of H_2O values observed in our study is larger than ranges observed in previous studies, likely a result of our more complete sampling. In addition, we are able to spatially resolve variation at the ~250 μm scale, which better enables our understanding of the processes that cause variations in hydration. Finally, though our mean and

median values overlap across the cores, we note that our values are likely more accurate because we better capture the full range of alteration and lithologies present in the ocean crust. We also calculate hydration in the correct volumetric proportions because the highly altered material is not under-sampled relative to the less altered crust.

In comparing our results to previous H_2O measurements of ocean gabbroic core sections, we find that our results are similar. Results from IODP Site 1309 on the Atlantis Massif measured H_2O ranging from 0.93 wt% to 12.71 wt%, consistent with the ranges we observed in the OmanDP cores (Blackman et al., 2006). The gabbros in Site 1309 range from 1.20 wt% to 3.10 wt% H_2O (Blackman et al., 2006), which are similar to the means of 3.2 wt% for the foliated and layered gabbros (Hole GT2A) and 2.8 wt% for the lower layered gabbros (Hole GT1A) that were calculated in our study. At another site, samples from Hole 1473A on the Atlantis Bank in the Indian Ocean were found to contain 0.2 – 8 wt% H_2O, with a mean of 1.0 ± 0.9 wt% H_2O (Macleod et al., 2017). In the nearby ODP Hole 735B, also on the Atlantis Bank of the Southwest Indian Ridge, H_2O contents range from 0 – 4 wt% H_2O, with a majority of the H_2O values falling between 0.5 – 2 wt% H_2O (Hertogen et al., 2002). Gabbroic rocks from Holes 894F-G at Hess Deep had LOI values ranging from 0.13 – 4.05 wt% (Lecuyer and Reynard, 1996). The overall ranges in these studies are broadly similar to our results, although each study only measured 99 to 451 samples.

Our results indicating that the lower gabbroic ocean crust is more hydrated than the sheeted dikes crust differ from previous estimates. However, we note that the lower sections of intact ocean crust formed at fast spreading rates, analogous to the Samail ophiolite, have not yet been sampled directly by ocean drilling. We attribute our results to two factors. First, the lower gabbroic ocean crust has experienced modestly less alteration than the upper sheeted dikes and gabbros, but the alteration phases formed at deeper depths have much higher wt% H_2O. Specifically, hydrothermal alteration processes that form large volumes of zeolite minerals are an important carrier of H_2O in the lower ocean crust. While the sheeted dikes and uppermost gabbros of the ocean crust (Hole GT3A) experienced more intense alteration, the greenschist facies alteration resulted in minerals with lower H_2O content, such as amphibole, and formed fewer high H_2O minerals than Holes GT1A and GT2A (Greenberger et al., 2021). Given that high frequencies of prehnite and zeolite are observed in GT2A and GT1A, which are deeper in the ocean crust, penetration of hydrothermal fluid is likely the cause of the lower temperature alteration occurring deeper in the ocean crust, as previously suggested (e.g., Heft et al., 2008; Alt et al., 2010; Wilson et al., 2006; Garrido et al., 2001; VanTongeren et al., 2008; Hanghøj et al., 2010; Dygert et al., 2017).

Second, throughout the lower gabbroic oceanic crust, veins and fault zones are present (see full maps in Files S1 – S2), and these zones have substantially increased hydration (Table 2; Figure 8). Faulting may enable fluid flow, which would increase alteration, and thus hydration, within and surrounding faulted areas. By design, a significant portion of the core from Hole GT1A sampled fault zones (~8%) that appear to be oceanic in origin (Kelemen et al., 2020; Zihlmann et al., 2018), though we note that additional later fault zones generated during obduction might also be contributing to hydration, unrelated to seafloor processes. Similarly, Coogan et al. (2006) estimated that such fault zones in the same block of the Samail ophiolite have 10 to 50 m widths with a spacing of ~ 1 km, thus comprising ~ 1 to 5 volume percent of the lower crust. Our results suggest that fault zones provide conduits for channeled fluid flow and locations for increased hydration and alteration within the deep ocean crust, supporting previous predictions. Because

fault zones appear to be a major driver of hydration within the ocean crust, hydration of any particular locale may be dependent on the local faulting and structure of the ocean crust in the region (Bruhn et al., 1994).

In applying these results to "typical" oceanic crust formed at fast-spreading ridges, several caveats should be considered. First, although the primitive lavas that formed the ophiolite had major element contents very similar to those of mid-ocean ridge basalts, trace element and geochronological data indicate that the crust of the Samail ophiolite formed via crystallization of hydrous magmas above a subduction zone, (e.g., Pearce et al., 1981; MacLeod et al., 2013; Rioux et al., 2016). Second, to the extent that the average water contents of core from Hole GT1A are influenced by the presence of highly altered fault zones, readers should keep in mind that the frequency and width of such zones have not yet been fully quantified for the Samail ophiolite, and are almost unknown for lower oceanic crust formed at intermediate- to fast-spreading, Pacific crust. Third, while OmanDP investigators have, like prior investigators of the Oman ophiolite (e.g. Kawahata et al., 2001; A'Shaikh et al., 2006, Pflumio et al., 1991), inferred that most of the low temperature, high H_2O-content alteration minerals in the core (i.e., zeolites) formed by water-rock reactions at or near the Samail spreading center, we did not do independent work to fully rule out the alternative that some of these minerals may have formed during or post-obduction.

High proportions of hydrous minerals within the crust influence the physical properties of the ocean crust. For example, the presence of faults, fractures, and damage zones have been demonstrated to impact seismic wave propagation (Berryman, 2007). The high levels of hydration in the lower oceanic crust and its fault zones relative to the rest of the crust may be related to the relatively low observed seismic wave speeds observed for oceanic lower crust, as compared to calculated wave speeds in fresh gabbro lithologies (Korenaga et al., 2002; Behn and Kelemen 2003). Our data on hydration as a function of depth can be used to update interpretations of seismic data for the ocean crust. In particular, the seismic wave speeds of zeolites have rarely if ever been considered in this context.

5 Conclusions

We quantified hydration of the ocean crust in drill core from the Samail ophiolite by developing a regression between geochemical measurements of LOI and spectral indices of OH/H_2O utilizing data from shortwave infrared micro-imaging spectroscopy of ICDP OmanDP Holes GT3A (sheeted dikes and upper gabbros), GT2A (middle ocean crust; foliated and layered gabbros), and the GT1A (lower ocean crust; layered gabbros). The integrated area of the OH/H_2O absorptions at ~1350 – 1650 nm in wavenumber determined H_2O wt. % concentrations with R^2 = 0.66 and a typical absolute accuracy of 0.52 ± 0.49 wt% H_2O. We applied our regression to each ~250-260 µm pixel in 1.2 km of rock core, comprising 1.07 billion pixels, to produce spatially resolved maps of ocean crust hydration.

Our results indicate that the majority of the ocean crust contains 0.5 – 3 wt% H_2O, and that overall ocean crust hydration ranges from 0 to ~18 wt% H_2O. Pixels sampling material with high H_2O occur where there is a higher prevalence of minerals with high H_2O contents (e.g., zeolites) while lower H_2O areas contain primary anhydrous mineralogy (pyroxene and plagioclase) and/or minerals with lower H_2O contents, such as amphibole. Hydration does increase to a certain degree

with extent of alteration, as expected, but the nature of the mineral phases formed as a result of alteration is an important determinant of bulk hydration of sections of the crust. Somewhat counterintuitively, we find the overall less altered lower crust is, in bulk, more hydrous by 1-2 wt. %, mainly due to the ubiquitous presence of H_2O-rich zeolites, together with localized, mineralized fault zones. The lowest mean H_2O (2.1 wt%) is in Hole GT3A, which experienced the most extensive alteration. Its secondary mineralogy is dominated by amphibole and epidote, relatively low wt% H_2O minerals, along with some chlorite. The mean H_2O wt. % contents in Holes GT2A (3.2 wt. %) and GT1A (2.8 wt. %) were considerably higher. Fault zones serve as conduits for the enhanced hydration of the lower ocean crust; gabbroic GT1A has relatively high levels of H_2O in fault zones (5.7 wt%), which are 2x as hydrated as the non-faulted regions of Hole GT1A (2.6 wt. % H_2O).

Overall, our ability to use the imaging spectroscopy dataset of the entire core, for a core with near 100% recovery, enables us to quantify H_2O in both the unaltered sections of the oceanic crust and the more altered sections that have been excluded from other studies, ultimately increasing estimates of bulk crustal hydration relative to previous work. The higher estimates for hydration of the lower ocean crust have implications for its rheologic properties in other processes.

Acknowledgements

Thanks to the scientific and technical staff of the Chikyu for facilitating acquisition of the imaging spectrometer data. This study used data from the Oman Drilling Project, which has been possible through co-mingled funds from the International Continental Scientific Drilling Project (ICDP; Kelemen, Matter, Teagle Lead PIs), the Sloan Foundation – Deep Carbon Observatory (Grant 2014-3-01, Kelemen PI), the National Science Foundation (NSF-EAR-1516300, Kelemen lead PI), NASA – Astrobiology Institute (NNA15BB02A, Templeton PI), the German Research Foundation (DFG: KO 1723/21-1, Koepke PI), the Japanese Society for the Promotion of Science (JSPS no:16H06347, Michibayashi PI; and KAKENHI 16H02742, Takazawa PI), the European Research Council (Adv: no.669972; Jamveit PI), the Swiss National Science Foundation (SNF:20FI21_163073, Früh-Green PI), JAMSTEC, the TAMU-JR Science Operator, and contributions from the Sultanate of Oman Ministry of Regional Municipalities and Water Resources, the Oman Public Authority of Mining, Sultan Qaboos University, CRNS-Univ. Montpellier II, Columbia University of New York, and the University of Southampton. BLE acknowledges a Rose Hills Foundation grant for supporting acquisition of the imaging spectroscopy data. MAC was supported by a George R. Rossman SURF fellowship at Caltech. We also thank NSF MG&G grant 2129700 to RG and BLE for supporting the completion of this work. We thank Natsue Abe for discussion of the implications of these results for the physical properties of the ocean crust. Finally, we thank Jeff Alt and one anonymous reviewer for their constructive reviews that improved the quality of this paper, and we thank Associate Editor Phil Janney and Editor Mark Dekkers for editorial handling.

The LOI measurements used in this study were published in Kelemen et al., (2020), and data are available from ICDP. The underlying imaging spectroscopy dataset used is archived through CaltechDATA (Greenberger et al., 2021, http://dx.doi.org/10.22002/D1.2009). H_2O maps of each core section are also available as PDF images (Crotteau et al., 2021, http://dx.doi.org/10.22002/D1.2141) and .img files through CaltechDATA (Crotteau et al., 2021,

http://dx.doi.org/10.22002/D1.2142). Regions of interest corresponding to the LOI samples are also archived on CaltechDATA (Crotteau et al., 2021, http://dx.doi.org/10.22002/D1.21412).

References

Agrinier, P., Hékinian, R., Bideau, D., & Javoy, M. (1995a). O and H stable isotope compositions of oceanic crust and upper mantle rocks exposed in the Hess Deep near the Galapagos Triple Junction. *Earth and Planetary Science Letters*, *136*(3–4), 183–196. https://doi.org/10.1016/0012-821X(95)00159-A

Agrinier, P., Laverne, C., & Tartarotti, P. (1995b). Stable isotope ratios (oxygen, hydrogen) and petrology of hydrothermally altered dolerites at the bottom of the sheeted dike complex of Hole 504B. *Proceedings of the Ocean Drilling Program, Scientific Results*, *140*. https://doi.org/10.2973/odp.proc.sr.137140.016.1995

Aines, R. D., & Rossman, G. R. (1984). Water in minerals? A peak in the infrared. *Journal of Geophysical Research: Solid Earth*, *89*(B6), 4059–4071. https://doi.org/10.1029/JB089iB06p04059

Alt, J. C., Kinoshita, H., Stokking, L. B., & Michael, P. J. (Eds.). (1996). *Proceedings of the Ocean Drilling Program, 148 Scientific Results* (Vol. 148). Ocean Drilling Program. https://doi.org/10.2973/odp.proc.sr.148.1996

Alt, J. C., Laverne, C., Coggon, R. M., Teagle, D. A. H., Banerjee, N. R., Morgan, S., et al., (2010). Subsurface structure of a submarine hydrothermal system in ocean crust formed at the East Pacific Rise, ODP/IODP Site 1256. *Geochemistry, Geophysics, Geosystems*, *11*(10). https://doi.org/10.1029/2010GC003144

Alt, J. C., & Teagle, D. A. H. (1999). The uptake of carbon during alteration of ocean crust. *Geochimica et Cosmochimica Acta*, *63*(10), 1527–1535. https://doi.org/10.1016/S0016-7037(99)00123-4

A'Shaikh, D. Matsueda, H., Mizuta, T., and Miyashita, S. (2006) Hydrothermal Alteration of Oman Ophiolite Extrusives in Ghuzayn Area. *Resource Geology* 56(2) 2, 167–182

Asimow, P. D., Stein, L. C., Mosenfelder, J. L., & Rossman, G. R. (2006). Quantitative polarized infrared analysis of trace OH in populations of randomly oriented mineral grains. *American Mineralogist*, *91*(2–3), 278–284. https://doi.org/10.2138/am.2006.1937

Behn, M. D., & Kelemen, P. B. (2003). Relationship between seismic P-wave velocity and the composition of anhydrous igneous and meta-igneous rocks. *Geochemistry, Geophysics, Geosystems*, *4*(5). https://doi.org/10.1029/2002GC000393

Bell, D. R., Ihinger, P. D., & Rossman, G. R. (1995). Quantitative analysis of trace OH in garnet and pyroxenes. *American Mineralogist*, *80*(5–6), 465–474. https://doi.org/10.2138/am-1995-5-607

Bell, D. R., Rossman, G. R., Maldener, J., Endisch, D., & Rauch, F. (2003). Hydroxide in olivine: A quantitative determination of the absolute amount and calibration of the IR spectrum. *Journal of Geophysical Research: Solid Earth*, *108*(B2). https://doi.org/10.1029/2001JB000679

Bell, David. R., Rossman, G. R., Maldener, J., Endisch, D., & Rauch, F. (2004). Hydroxide in kyanite: A quantitative determination of the absolute amount and calibration of the IR spectrum. *American Mineralogist*, *89*(7), 998–1003. https://doi.org/10.2138/am-2004-0710

Berryman, J. G. (2007). Seismic waves in rocks with fluids and fractures. *Geophysical Journal International*, *171*(2), 954–974. https://doi.org/10.1111/j.1365-246X.2007.03563.x

Blacic, J. D. (1972). Effect of Water on the Experimental Deformation of Olivine. In *Flow and Fracture of Rocks* (pp. 109–115). American Geophysical Union (AGU). https://doi.org/10.1029/GM016p0109

Blackman, D. K., Ildefonse, B., John, B. E., Ohara, Y., Miller, D. J., MacLeod, C. J., & The Expedition 304/305 Scientists (Eds.). (2006). *Proceedings of the IODP, 304/305* (Vol. 302). Integrated Ocean Drilling Program. https://doi.org/10.2204/iodp.proc.304305.2006

Bruhn, R. L., Parry, W. T., Yonkee, W. A., & Thompson, T. (1994). Fracturing and hydrothermal alteration in normal fault zones. *Pure and Applied Geophysics*, *142*(3), 609–644. https://doi.org/10.1007/BF00876057

Burns, R. G. (1993). Mineralogical applications of crystal field theory. Cambridge University Press.

Campbell, I. H., & Taylor, S. R. (1983). No water, no granites - No oceans, no continents. *Geophysical Research Letters*, *10*(11), 1061–1064. https://doi.org/10.1029/GL010i011p01061

Chopra, P. N., & Paterson, M. S. (1984). The role of water in the deformation of dunite. *Journal of Geophysical Research: Solid Earth*, *89*(B9), 7861–7876. https://doi.org/10.1029/JB089iB09p07861

Clark, R. N., King, T. V. V., Klejwa, M., Swayze, G. A., & Vergo, N. (1990). High spectral resolution reflectance spectroscopy of minerals. *Journal of Geophysical Research: Solid Earth*, *95*(B8), 12653–12680. https://doi.org/10.1029/JB095iB08p12653

Clark, R. N., Swayze, G. A., Livo, K. E., Kokaly, R. F., Sutley, S. J., Dalton, J. B., et al., (2003). Imaging spectroscopy: Earth and planetary remote sensing with the USGS Tetracorder and expert systems. *Journal of Geophysical Research: Planets*, *108*(E12). https://doi.org/10.1029/2002JE001847

Coggon, R. M., Teagle, D. A. H., Harris, M., Davidson, G. J., Alt, J. C., & Brewer, T. S. (2016). Hydrothermal contributions to global biogeochemical cycles: Insights from the Macquarie Island ophiolite. *Lithos*, *264*, 329–347. https://doi.org/10.1016/j.lithos.2016.08.024

Coogan, L. A., Howard, K. A., Gillis, K. M., Bickle, M. J., Chapman, H., Boyce, A. J., et al., (2006). Chemical and thermal constraints on focussed fluid flow in the lower oceanic crust. *American Journal of Science*, *306*(6), 389–427. https://doi.org/10.2475/06.2006.01

Crotteau, M. A., Greenberger, R. N., Ehlmann, B. L., Rossman, G. R., Harris, M., Kelemen, P. B., et al. (2021). Hydration Imaging Spectroscopy Dataset for Oman Drilling Project Holes GT1A, GT2A, and GT3A (Version 1.0) [Data set]. CaltechDATA. https://doi.org/10.22002/D1.2142

Crotteau, M. A., Greenberger, R. N., Ehlmann, B. L., Rossman, G. R., Harris, M., Kelemen, P. B., et al. (2021). Hydration Maps of Oman Drilling Project Holes GT1A, GT2A, and GT3A (Version 1.0) [Data set]. CaltechDATA. https://doi.org/10.22002/D1.2141

Dygert, N., Kelemen, P. B., & Liang, Y. (2017). Spatial variations in cooling rate in the mantle section of the Samail ophiolite in Oman: Implications for formation of lithosphere at mid-ocean ridges. *Earth and Planetary Science Letters, 465*, 134–144. https://doi.org/10.1016/j.epsl.2017.02.038

Früh-Green, G. L., Plas, A., & Lécuyer, C. (1996). Petrologic and Stable Isotope Constraints on Hydrothermal Alteration and Serpentinization of the EPR Shallow Mantle at Hess Deep (Site 895). In *Proc. Ocean Drill. Program Sci. Results* (Vol. 147). https://doi.org/10.2973/odp.proc.sr.147.016.1996

Garrido, C. J., Kelemen, P. B., & Hirth, G. (2001). Variation of cooling rate with depth in lower crust formed at an oceanic spreading ridge: Plagioclase crystal size distributions in gabbros from the Oman ophiolite. *Geochemistry, Geophysics, Geosystems, 2*(10). https://doi.org/10.1029/2000GC000136

Glennie, K. W., Boeuf, M. G. A., Clarke, M. W. H., Moody-Stuart, M., Pilaar, W. F. H., & Reinhardt, B. M. (1973). Late Cretaceous Nappes in Oman Mountains and Their Geologic Evolution. *AAPG Bulletin*, 57(1), 5–27.

Godard, M., Awaji, S., Hansen, H., Hellebrand, E., Brunelli, D., Johnson, K., et al., (2009). Geochemistry of a long in-situ section of intrusive slow-spread oceanic lithosphere: Results from IODP Site U1309 (Atlantis Massif, 30°N Mid-Atlantic-Ridge). *Earth and Planetary Science Letters, 279*(1), 110–122. https://doi.org/10.1016/j.epsl.2008.12.034

Greenberger, R. N. Harris, M., Ehlmann, B. L., Crotteau, M. A., Kelemen, P. B., Manning, C. E., Teagle, D. A. H., and the Oman Drilling Project Science Party (2021), Hydrothermal Alteration of the Ocean Crust and Patterns in Mineralization with Depth as Measured by Micro-Imaging Infrared Spectroscopy, *Journal of Geophysical Research – Solid Earth, 126*, e2021JB021976. doi: 10.1029/2021JB021976

Greenberger, R. N., Ehlmann, B. L., & the Oman Drilling Project Science Party. (2021). Oman Drilling Project micro-imaging spectroscopy data. CaltechDATA. https://doi.org/10.22002/D1.2009

Hacker, B. R. (2008). H_2O subduction beyond arcs. *Geochemistry, Geophysics, Geosystems, 9*(3). https://doi.org/10.1029/2007GC001707

Hammer, V. M. F., Beran, A., Endisch, D., & Rauch, F. (1996). OH concentrations in natural titanites determined by FTIR spectroscopy and nuclear reaction analysis. *European Journal of Mineralogy*, 281–288. https://doi.org/10.1127/ejm/8/2/0281

Hanghøj, K., Kelemen, P. B., Hassler, D., & Godard, M. (2010). Composition and Genesis of Depleted Mantle Peridotites from the Wadi Tayin Massif, Oman Ophiolite; Major and Trace Element Geochemistry, and Os Isotope and PGE Systematics. *Journal of Petrology, 51*(1–2), 201–227. https://doi.org/10.1093/petrology/egp077

Hapke, B. (2012). Theory of Reflectance and Emittance Spectroscopy. Cambridge University Press.

Harris, M., Coggon, R. M., Smith-Duque, C. E., Cooper, M. J., Milton, J. A., & Teagle, D. A. H. (2015). Channelling of hydrothermal fluids during the accretion and evolution of the upper oceanic crust: Sr isotope evidence from ODP Hole 1256D. *Earth and Planetary Science Letters*, *416*, 56–66. https://doi.org/10.1016/j.epsl.2015.01.042

Heft, K. L., Gillis, K. M., Pollock, M. A., Karson, J. A., & Klein, E. M. (2008). Role of upwelling hydrothermal fluids in the development of alteration patterns at fast spreading ridges: Evidence from the sheeted dike complex at Pito Deep. *Geochemistry, Geophysics, Geosystems, 9*(5). https://doi.org/10.1029/2007GC001926

Hertogen, J., Emmermann, R., Robinson, P.T., and Erzinger, J. (2002). Lithology, mineralogy, and geochemistry of the lower ocean crust, ODP Hole 735B, Southwest Indian Ridge. In Natland, J.H., Dick, H.J.B., Miller, D.J., and Von Herzen, R.P. (Eds.), Proc. ODP, Sci. Results, 176: College Station, TX (Ocean Drilling Program), 1–82. https://doi:10.2973/odp.proc.sr.176.003.2002

Hunt, G. R. (1977). Spectral signatures of particulate minerals in the visible and near infrared. *Geophysics*, *42*(3), 501–513. https://doi.org/10.1190/1.1440721

Jamtveit, B., Brooker, R., Brooks, K., Larsen, L. M., & Pedersen, T. (2001). The water content of olivines from the North Atlantic Volcanic Province. *Earth and Planetary Science Letters*, *186*(3), 401–415. https://doi.org/10.1016/S0012-821X(01)00256-4

Jarrard, R. D. (2003). Subduction fluxes of water, carbon dioxide, chlorine, and potassium. *Geochemistry, Geophysics, Geosystems*, *4*(5). https://doi.org/10.1029/2002GC000392

Johnson, E. A., & Rossman, G. R. (2003). The concentration and speciation of hydrogen in feldspars using FTIR and 1H MAS NMR spectroscopy. *American Mineralogist*, *88*(5–6), 901–911. https://doi.org/10.2138/am-2003-5-620

Kawahata, H., Kusakabe, M., & Kikuchi, Y. (1987). Strontium, oxygen, and hydrogen isotope geochemistry of hydrothermally altered and weathered rocks in DSDP Hole 504B, Costa Rica Rift. *Earth and Planetary Science Letters*, *85*(4), 343–355. https://doi.org/10.1016/0012-821X(87)90132-4

Kawahata, H., Nohara, M., Ishizuka, H., Hasebe, S., & Chiba, H. (2001). Sr isotope geochemistry and hydrothermal alteration of the Oman ophiolite. Journal of Geophysical Research, 106, 11083– 11099. https://doi.org/10.1029/2000jb900456

Kelemen, P. B., Koga, K., & Shimizu, N. (1997). Geochemistry of gabbro sills in the crust-mantle transition zone of the Oman ophiolite: implications for the origin of the oceanic lower crust. *Earth and Planetary Science Letters*, *146*(3), 475–488. https://doi.org/10.1016/S0012-821X(96)00235-X

Kelemen, P. (2013). Planning the Drilling of the Samail Ophiolite in Oman. *Eos, Transactions American Geophysical Union*, *94*(3), 32–32. https://doi.org/10.1002/2013EO030008

Kelemen, P., Al Rajhi, A., Godard, M., Ildefonse, B., Köpke, J., MacLeod, C., et al., (2013). Scientific Drilling and Related Research in the Samail Ophiolite, Sultanate of Oman. *Scientific Drilling*, *15*, 64–71. https://doi.org/10.2204/iodp.sd.15.10.2013

Kelemen, P. B., Matter, J. M., Teagle, D. A. H., Coggon, J. A., & Oman Drilling Project Science Team. (2020). *Proceedings of the Oman Drilling Project: Scientific Drilling in the*

Samail Ophiolite, Sultanate of Oman (Vol. Phase 1 and 2). International Ocean Discovery Program. https://doi.org/10.14379/OmanDP.proc.2020

Kleine, B. I., Stefánsson, A., Halldórsson, S. A., & Barnes, J. D. (2020). Impact of fluid-rock interaction on water uptake of the Icelandic crust: Implications for the hydration of the oceanic crust and the subducted water flux. *Earth and Planetary Science Letters*, *538*, 116210. https://doi.org/10.1016/j.epsl.2020.116210

Korenaga, J., Kelemen, P. B., & Holbrook, W. S. (2002). Methods for resolving the origin of large igneous provinces from crustal seismology: LARGE IGNEOUS PROVINCES AND SEISMOLOGY. *Journal of Geophysical Research: Solid Earth*, *107*(B9), ECV 1-1-ECV 1-27. https://doi.org/10.1029/2001JB001030

Kusakabe, M., Shibata, T., Yamamoto, M., Mayeda, S., Kagami, H., Honma, H., et al., (1989). Petrology and isotope characteristics (H, O, S, Sr and Nd) of basalts from ocean drilling program Hole 504B, Leg 111, Costa Rica Rift. Proc., *Scientific Results, ODP, Leg 111, Costa Rica Rift*. https://doi.org/10.2973/odp.proc.sr.111.115.1989

Lechler, P. J., & Desilets, M. O. (1987). A review of the use of loss on ignition as a measurement of total volatiles in whole-rock analysis. *Chemical Geology*, *63*(3–4), 341–344. https://doi.org/10.1016/0009-2541(87)90171-9

Lecuyer, C., & Reynard, B. (1996). High-temperature alteration of oceanic gabbros by seawater (Hess Deep, Ocean Drilling Program Leg 147): Evidence from oxygen isotopes and elemental fluxes. *Journal of Geophysical Research: Solid Earth*, *101*(B7), 15883–15897. https://doi.org/10.1029/96JB00950

Libowitzky, E., & Rossman, G. R. (1996). Principles of quantitative absorbance measurements in anisotropic crystals. *Physics and Chemistry of Minerals*, *23*(6), 319–327. https://doi.org/10.1007/BF00199497

Libowitzky, E., & Rossman, G. R. (1997). An IR absorption calibration for water in minerals. *American Mineralogist*, *82*(11–12), 1111–1115. https://doi.org/10.2138/am-1997-11-1208

MacLeod, C. J., Johan Lissenberg, C., & Bibby, L. E. (2013). "Moist MORB" axial magmatism in the Oman ophiolite: The evidence against a mid-ocean ridge origin. *Geology*, *41*(4), 459–462. https://doi.org/10.1130/G33904.1

MacLeod, C.J., Dick, H.J.B., Blum, P., and the Expedition 360 Scientists (2017). *Proceedings of the International Ocean Discovery Program* (Vol. 360). doi:10.14379/iodp.proc.360.103.2017

Michibayashi, K., Tominaga, M., Ildefonse, B., & Teagle, D. (2019). What Lies Beneath: The Formation and Evolution of Oceanic Lithosphere. *Oceanography*, *32*(1), 138–149. https://doi.org/10.5670/oceanog.2019.136

Milliken, R. E., & Mustard, J. F. (2005). Quantifying absolute water content of minerals using near-infrared reflectance spectroscopy. *Journal of Geophysical Research: Planets*, *110*(E12). https://doi.org/10.1029/2005JE002534

Milliken, R. E., & Mustard, J. F. (2007). Estimating the water content of hydrated minerals using reflectance spectroscopy: I. Effects of darkening agents and low-albedo materials. *Icarus*, *189*(2), 550–573. https://doi.org/10.1016/j.icarus.2007.02.017

Milliken, R. E., & Mustard, J. F. (2007). Estimating the water content of hydrated minerals using reflectance spectroscopy: II. Effects of particle size. *Icarus*, *189*(2), 574–588. https://doi.org/10.1016/j.icarus.2006.12.028

Moores, E. M., & F J. Vine, F. J. (1971). The Troodos Massif, Cyprus and other ophiolites as oceanic crust: evaluation and implications. *Philosophical Transactions of the Royal Society of London. Series A, Mathematical and Physical Sciences*, *268*(1192), 443–467. https://doi.org/10.1098/rsta.1971.0006

Müller, R. D., & Dutkiewicz, A. (2018). Oceanic crustal carbon cycle drives 26-million-year atmospheric carbon dioxide periodicities. *Science Advances*, *4*(2), eaaq0500. https://doi.org/10.1126/sciadv.aaq0500

Pearce, J. A., Alabaster, T., Shelton, A. W., Searle, M. P., Vine, F. J., & Smith, A. G. (1981). The Oman ophiolite as a Cretaceous arc-basin complex: evidence and implications. *Philosophical Transactions of the Royal Society of London. Series A, Mathematical and Physical Sciences*, *300*(1454), 299–317. https://doi.org/10.1098/rsta.1981.0066

Pflumio, C. (1991), Evidences for polyphased oceanic alteration of the extrusive sequence of the Semail Ophiolite from the Salahi Block (northern Oman), in Ophiolite Genesis and Evolution of the Oceanic Lithosphere, edited by T. Peters, A. Nicolas, and R. J. Coleman, pp. 313– 351, Kluwer Acad., Norwell, Mass.

Potter, R. M., & Rossman, G. R. (1979). The tetravalent manganese oxides: identification, hydration, and structural relationships by infrared spectroscopy. *American Mineralogist*, *64*(11–12), 1199–1218.

Rossman, G. R. (2006). Analytical Methods for Measuring Water in Nominally Anhydrous Minerals. *Reviews in Mineralogy and Geochemistry*, *62*(1), 1–28. https://doi.org/10.2138/rmg.2006.62.1

Rioux, M., Bowring, S., Kelemen, P., Gordon, S., Dudás, F., & Miller, R. (2012). Rapid crustal accretion and magma assimilation in the Oman-U.A.E. ophiolite: High precision U-Pb zircon geochronology of the gabbroic crust. *Journal of Geophysical Research: Solid Earth*, *117*(B7). https://doi.org/10.1029/2012JB009273

Rioux, M., Garber, J., Bauer, A., Bowring, S., Searle, M., Kelemen, P., & Hacker, B. (2016). Synchronous formation of the metamorphic sole and igneous crust of the Semail ophiolite: New constraints on the tectonic evolution during ophiolite formation from high-precision U–Pb zircon geochronology. *Earth and Planetary Science Letters*, *451*, 185–195. https://doi.org/10.1016/j.epsl.2016.06.051

Schuttlefield, J. D., Cox, D., & Grassian, V. H. (2007). An investigation of water uptake on clays minerals using ATR-FTIR spectroscopy coupled with quartz crystal microbalance measurements. *Journal of Geophysical Research: Atmospheres*, *112*(D21). https://doi.org/10.1029/2007JD008973

Searle, M., & Cox, J. (1999). Tectonic setting, origin, and obduction of the Oman ophiolite. *GSA Bulletin*, *111*(1), 104–122. https://doi.org/10.1130/0016-7606(1999)111<0104:TSOAOO>2.3.CO;2

Shilobreeva, S., Martinez, I., Busigny, V., Agrinier, P., & Laverne, C. (2011). Insights into C and H storage in the altered oceanic crust: Results from ODP/IODP Hole 1256D. *Geochimica et Cosmochimica Acta*, *75*(9), 2237–2255. https://doi.org/10.1016/j.gca.2010.11.027

Shuai, K., & Yang, X. (2017). Quantitative analysis of H-species in anisotropic minerals by polarized infrared spectroscopy along three orthogonal directions. *Contributions to Mineralogy and Petrology*, *172*(2–3). https://doi.org/10.1007/s00410-017-1336-2

Skogby, H., Bell, D.R., Rossman, G.R. (1990) Hydroxide in pyroxenes: variations in the natural environment. *American Mineralogist* 75, 764-774.

Stolper, E. (1982). Water in silicate glasses: An infrared spectroscopic study. *Contributions to Mineralogy and Petrology*, *81*(1), 1–17. https://doi.org/10.1007/BF00371154

Sunshine, J. M., Pieters, C. M., & Pratt, S. F. (1990). Deconvolution of mineral absorption bands: An improved approach. *Journal of Geophysical Research: Solid Earth*, *95*(B5), 6955–6966. https://doi.org/10.1029/JB095iB05p06955

Teagle, D., Ildefonse, B., & Blum, P. (2012). *Proceedings Integrated Ocean Drilling Program, 335*. IODP. https://doi.org/10.2204/iodp.proc.335.2012

Tilton, G. R., Hopson, C. A., & Wright, J. E. (1981). Uranium-lead isotopic ages of the Samail Ophiolite, Oman, with applications to Tethyan ocean ridge tectonics. *Journal of Geophysical Research: Solid Earth*, *86*(B4), 2763–2775. https://doi.org/10.1029/JB086iB04p02763

Tominaga, M., Teagle, D. A. H., Alt, J. C., & Umino, S. (2009). Determination of the volcanostratigraphy of oceanic crust formed at superfast spreading ridge: Electrofacies analyses of ODP/IODP Hole 1256D. *Geochemistry, Geophysics, Geosystems, 10*(1). https://doi.org/10.1029/2008GC002143

VanTongeren, J. A., Kelemen, P. B., & Hanghøj, K. (2008). Cooling rates in the lower crust of the Oman ophiolite: Ca in olivine, revisited. *Earth and Planetary Science Letters, 267*(1–2), 69–82. https://doi.org/10.1016/j.epsl.2007.11.034

White, A. J. R., Laukamp, C. Stokes, M. A., Legras, M., Pejcic, B. (2017). Vibrational spectroscopy of epidote, pumpellyite and prehnite applied to low-grade regional metabasites. *Geochemistry: Exploration, Environment, Analysis, 17*(4), 315–333. https://doi.org/10.1144/geochem2016-007

Wilson, D. S., Teagle, D. A. H., Alt, J. C., Banerjee, N. R., Umino, S., Miyashita, S., et al., (2006). Drilling to Gabbro in Intact Ocean Crust. *Science*, *312*(5776), 1016–1020. https://doi.org/10.1126/science.1126090

Zihlmann, B., Müller, S., Coggon, R. M., Koepke, J., Garbe-Schönberg, D., & Teagle, D. A. H. (2018). Hydrothermal fault zones in the lower oceanic crust: An example from Wadi Gideah, Samail ophiolite, Oman. *Lithos, 323*, 103–124. https://doi.org/10.1016/j.lithos.2018.09.008

Figure Captions

Figure 1. Stratigraphic section (left) and geologic map (right) of the OmanDP boreholes. Boreholes considered in this study are outlined in red. Adapted from Kelemen et al., (2020).

Figure 2. Three example spectra showing the impacts of smoothing and continuum removal on the calculation of integrated area for single pixels. (a, d, g) The high hydration example is a pixel from Hole GT1A, Section 140Z-2. (b, e, h) The medium hydration sample is a pixel from Hole GT2A, Section 31Z-1. (c, f, i) The low hydration example is a pixel from Hole GT2A, Section 108Z-1. (a-c) Reflectance spectra. (d-f) Reflectance spectra at wavelengths used in final regression. (g-i) Continuum removed spectra at wavelengths used in final regression. The shaded region represents the integrated area calculated for each pixel. H_2O (pixel, IR) corresponds to the calculated wt% H_2O calculated based on the integrated area of the smoothed IR spectrum for the single pixels shown in (a-i) using equation 1. H_2O (sample, LOI) gives the measured H_2O from loss on ignition (LOI) for the entire ROI representing the sampled area. The single pixel is located within the ROI. Minor differences between the smoothed and unsmoothed spectra may occur due variability within the surrounding pixels.

Figure 3. Results from each set of parameters for the area calculations: (a) Integrated area of the H_2O combination absorption at 1900 nm calculated in wavelength space versus H_2O measured via LOI; (b) Integrated area of the H_2O combination absorption at 1900 nm calculated in wavenumber space versus H_2O measured via LOI. (c) Integrated area of the ~1400 nm H_2O/OH absorptions calculated in wavelength space versus H_2O measured via LOI. (d) Integrated area of the ~1400 nm H_2O/OH absorptions calculated in wavenumber space versus H_2O measured via LOI. Gray circles are outliers and rare rock types excluded from the regression.

Figure 4. Example of hydration maps (right) shown with standard color scans of core sections from the multi-sensor core logger (Kelemen et al., 2020). Approximate location sampled for geochemical analysis is outlined in a rectangular box on the hydration image (left). (a) A high hydration sample from Hole GT1A, Section 140Z-2 (LOI H_2O = 5.9 wt%; spectral estimate 7.2 wt%). (b) A medium hydration sample Hole GT2A, Section 31Z-1 (LOI H_2O = 3.1 wt%; spectral estimate 3.3 wt%). (c) A low hydration sample from Hole GT2A, Section 108Z-1 (LOI H_2O = 0.0 wt%; spectral estimate 0.7 wt%).

Figure 5. Downhole plots of calculated wt% H_2O versus depth for Holes GT3A, GT2A, and GT1A. 1 meter averages of calculated wt% H_2O are shown in black, and 10 centimeter averages of calculated wt% H_2O are shown in light gray. For comparison, red dots are the wt% H_2O of samples with LOI measurements. The main fault zones in GT1A are marked in yellow from Kelemen et al., (2020). Major fault zones were only identified and described for Hole GT1A, so we only consider fault zones from GT1A here. All fault zones regardless of size were grouped for Holes GT3A and GT2A.

Figure 6. Histograms of calculated wt% H_2O content for pixels in Holes GT3A, GT2A, and GT1A. All values greater than or equal to 15 wt% calculated H_2O were combined into one bin.

Figure 7. A comparison between the spatial occurrence frequency of a mineral (the percentage of pixels in which the mineral occurs) within each meter of core versus the mean calculated H_2O

in that meter. The relationships between the spatial occurrence frequency of (a) pyroxene, (b) chlorite, (c) prehnite, (d) zeolite, and (e) epidote versus calculated wt% H_2O. **Figure 8.** Calculated H_2O weight percent for pixels within the fault zones for GT1A versus those outside the major fault zones of GT1A. Major fault zones compose ~8.3% of Hole GT1A (Kelemen et al., 2020). The total number of pixels including in each of the histograms is given by n.

Table 1. Mean, median, and standard deviation of calculated weight percent H_2O values for holes GT3A, GT2A, and GT1A using imaging spectroscopy and, for comparison, the LOI geochemistry measurements (Kelemen et al., 2020).

Hole	**H_2O (wt%) from spectroscopy**			**H_2O (wt%) from LOI samples**			
	Mean	**Median**	**Standard Deviation**	**# of Samples**	**Mean H_2O**	**Median H_2O**	**Standard deviation**
GT3A (dike – gabbro transition)	2.1	1.7	1.6	64	1.7	1.5	0.8
GT2A (foliated and layered gabbros)	3.2	2.2	3.0	43	2.2	2.0	1.5
GT1A (layered gabbros)	2.8	1.5	3.1	34	2.2	1.6	2.0

Table 2. H_2O wt% inside and outside of fault zones in GT1A, measured by the spectral index.

	Mean H_2O (wt%)	**Median H_2O (wt%)**	**Standard Deviation (wt%)**
All GT1A	2.8	1.5	3.1
In fault zones	5.7	4.7	4.0
Out of fault zones	2.6	1.3	2.9

Note: Depths corresponding to fault zones are 21.00 m – 24.85 m, 84.14 m – 87.62, 161.20 m – 162.16 m, 164.2 m – 165.84 m, 168.60 m – 170.29 m, 172.27 m – 173.33 m, 190.59 m – 194.24 m, 200.20 m – 201.98 m, 213.95 – 216.81 m, 272.59 m – 275.13 m, 329.05 m – 333.85 m, and 336.03 m – 340.40 m (Kelemen et al., 2020).

Sediments
Lavas
Sheeted Dykes
Vari-textured Gabbros
Plagiogranite
Foliated Gabbros
Layered Gabbros
Tectonised
Mantle Peridotites
Dunites

GT3
GT2
GT1
CM1&2
BA1-4
BT1

Depth (km)
0
1
2
3
4
5
6
7
8
~10
~15
~20

Crust-Mantle
Transition

Crust
Mantle

24°00'
0 20 40km
58°00'
24°00'

City/Town
OmanDP drill site
Gabbros & extrusives
Peridotites
Metamorphic sole
Hawasina formation

Al Suwayq
Barka
Muscat
Rustaq
Al Hajar
JEBEL AKHDAR
Samail
Nizwa
Ibra

BT1
GT3
CM1 & 2
GT1
GT2
BA2
BA1,3,4

23°00'
23°00'
57°00'
58°00'

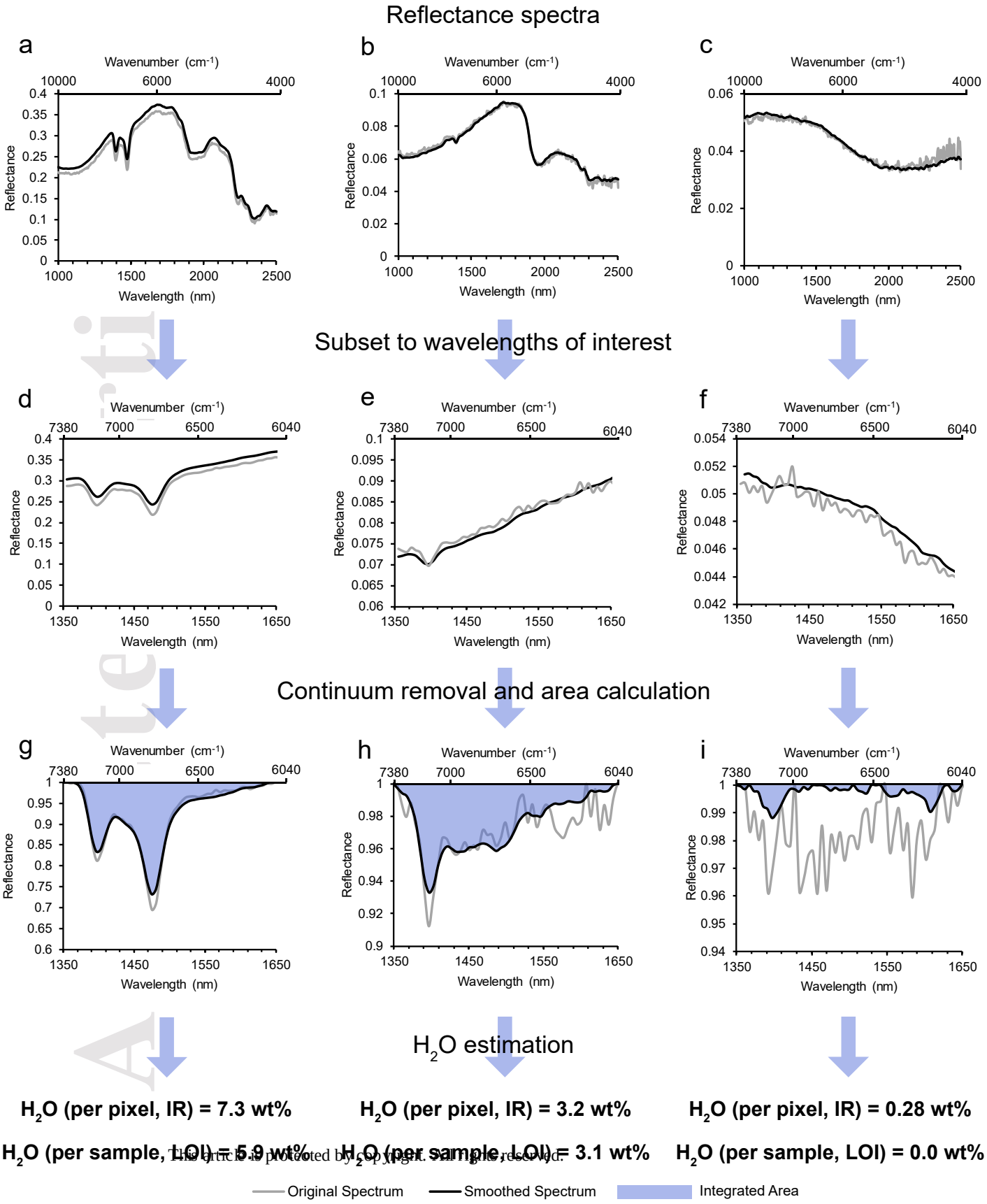

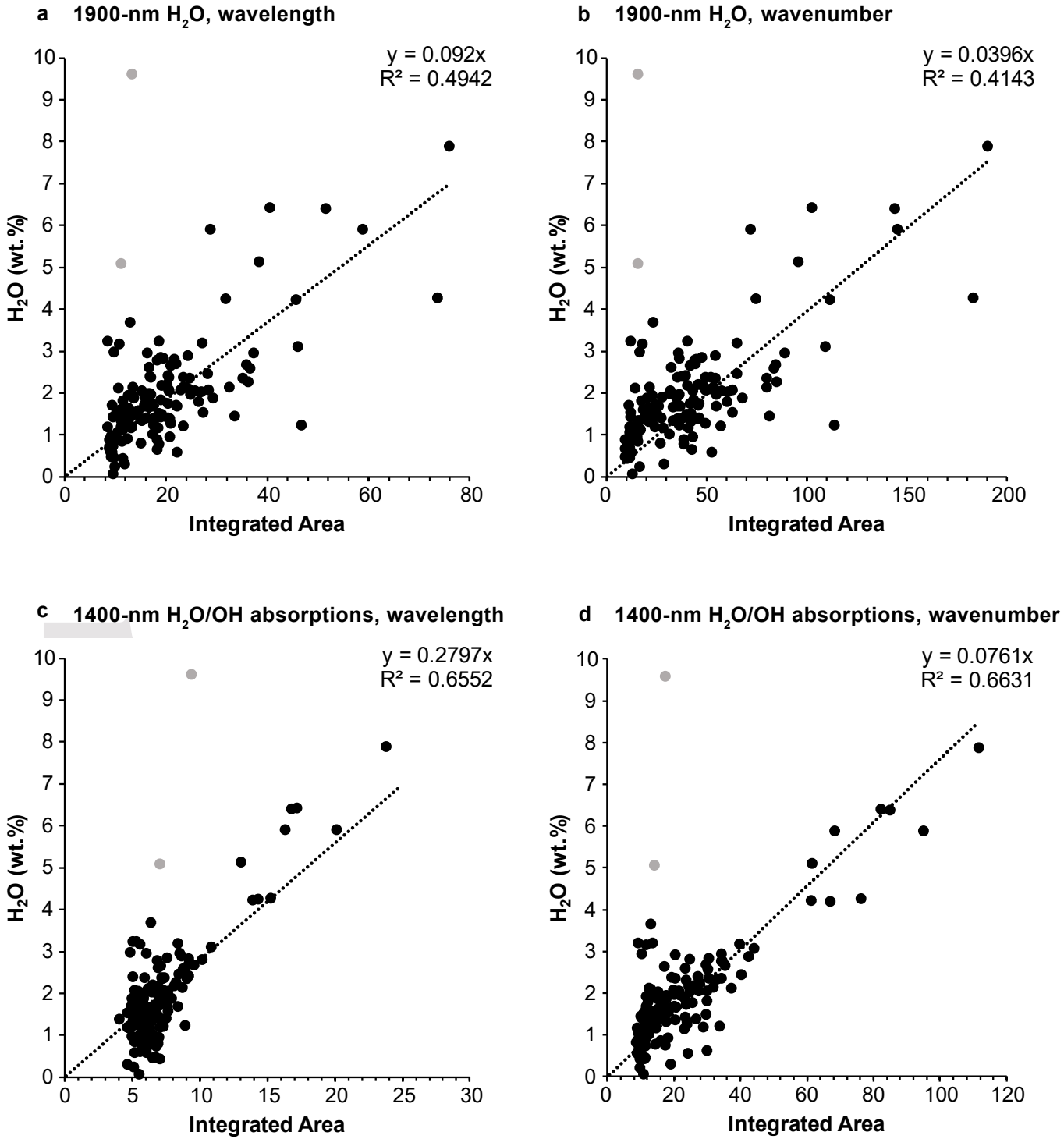

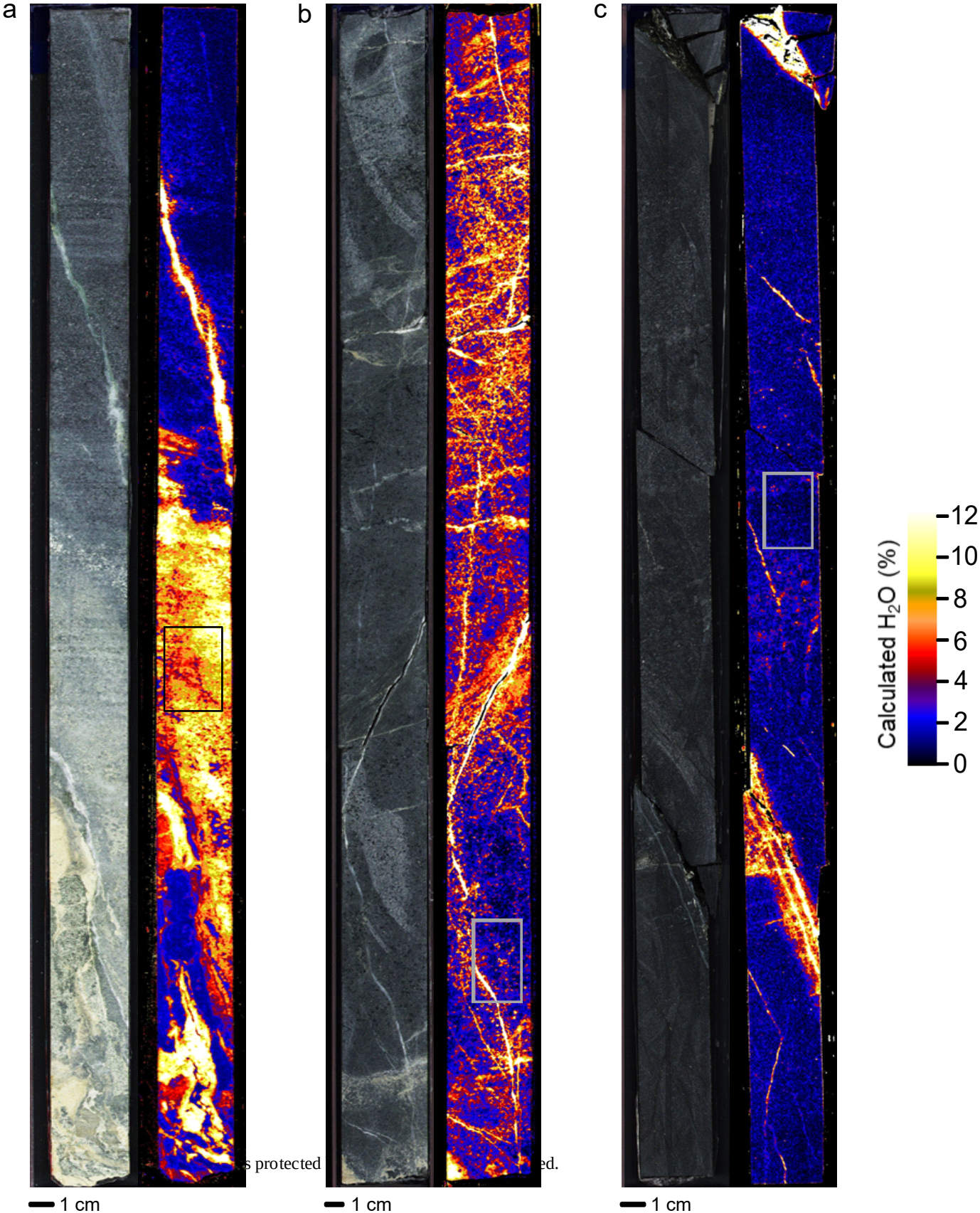

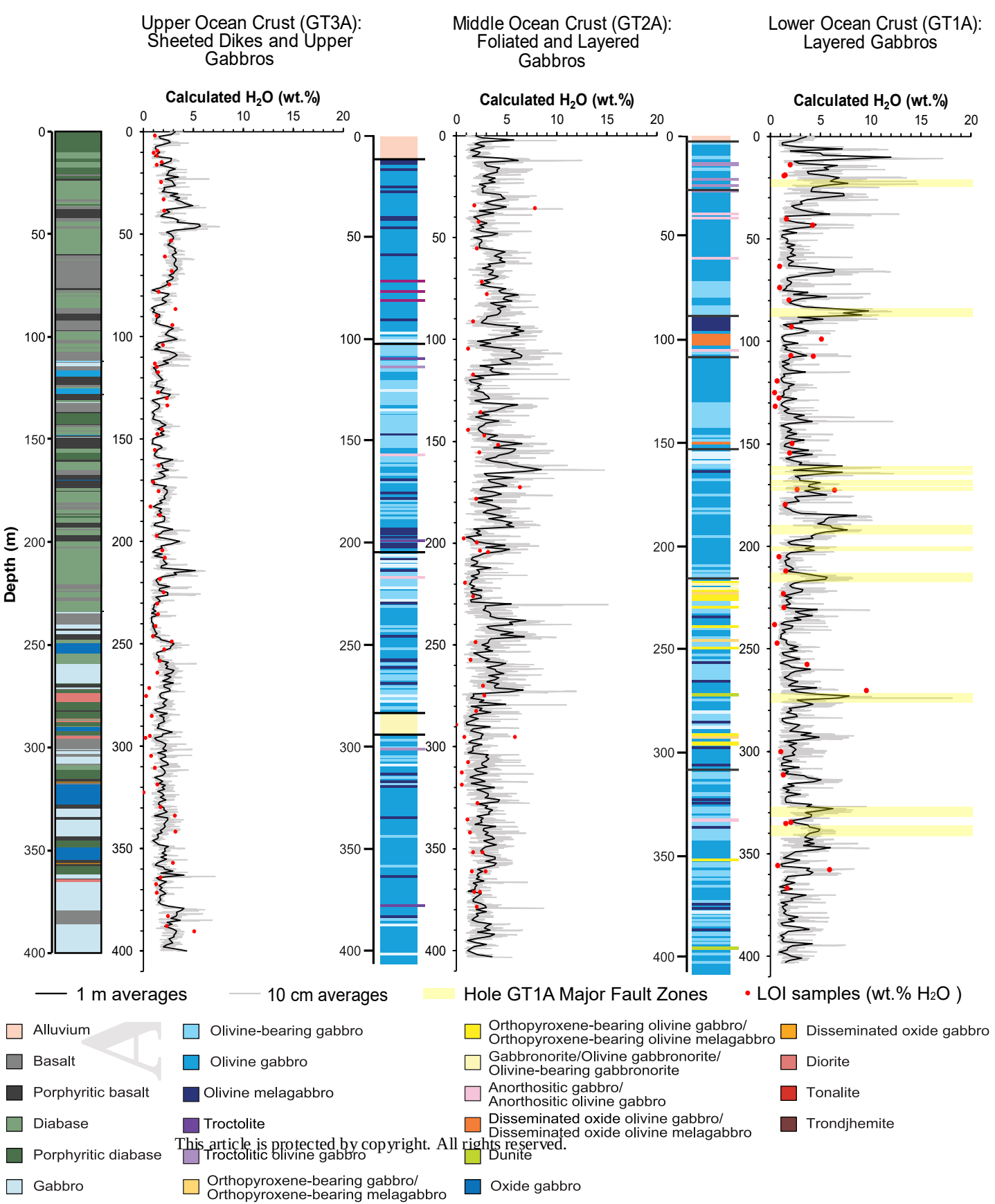

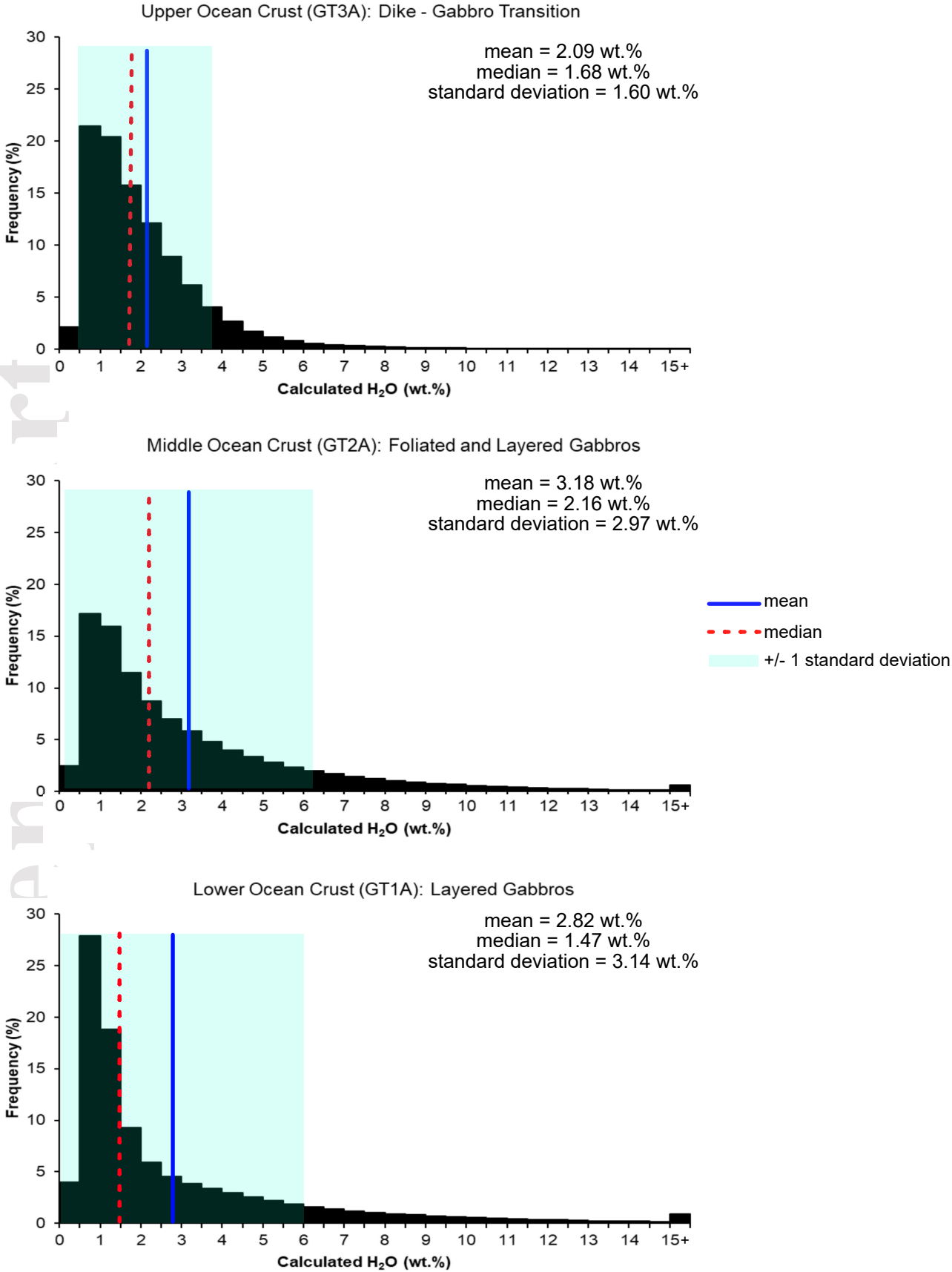
Upper Ocean Crust (GT3A): Dike - Gabbro Transition
mean = 2.09 wt.%
median = 1.68 wt.%
standard deviation = 1.60 wt.%
Frequency (%)
Calculated H2O (wt.%)
Middle Ocean Crust (GT2A): Foliated and Layered Gabbros
mean = 3.18 wt.%
median = 2.16 wt.%
standard deviation = 2.97 wt.%
Frequency (%)
Calculated H2O (wt.%)
mean
median
+/- 1 standard deviation
Lower Ocean Crust (GT1A): Layered Gabbros
mean = 2.82 wt.%
median = 1.47 wt.%
standard deviation = 3.14 wt.%
Frequency (%)
Calculated H2O (wt.%)

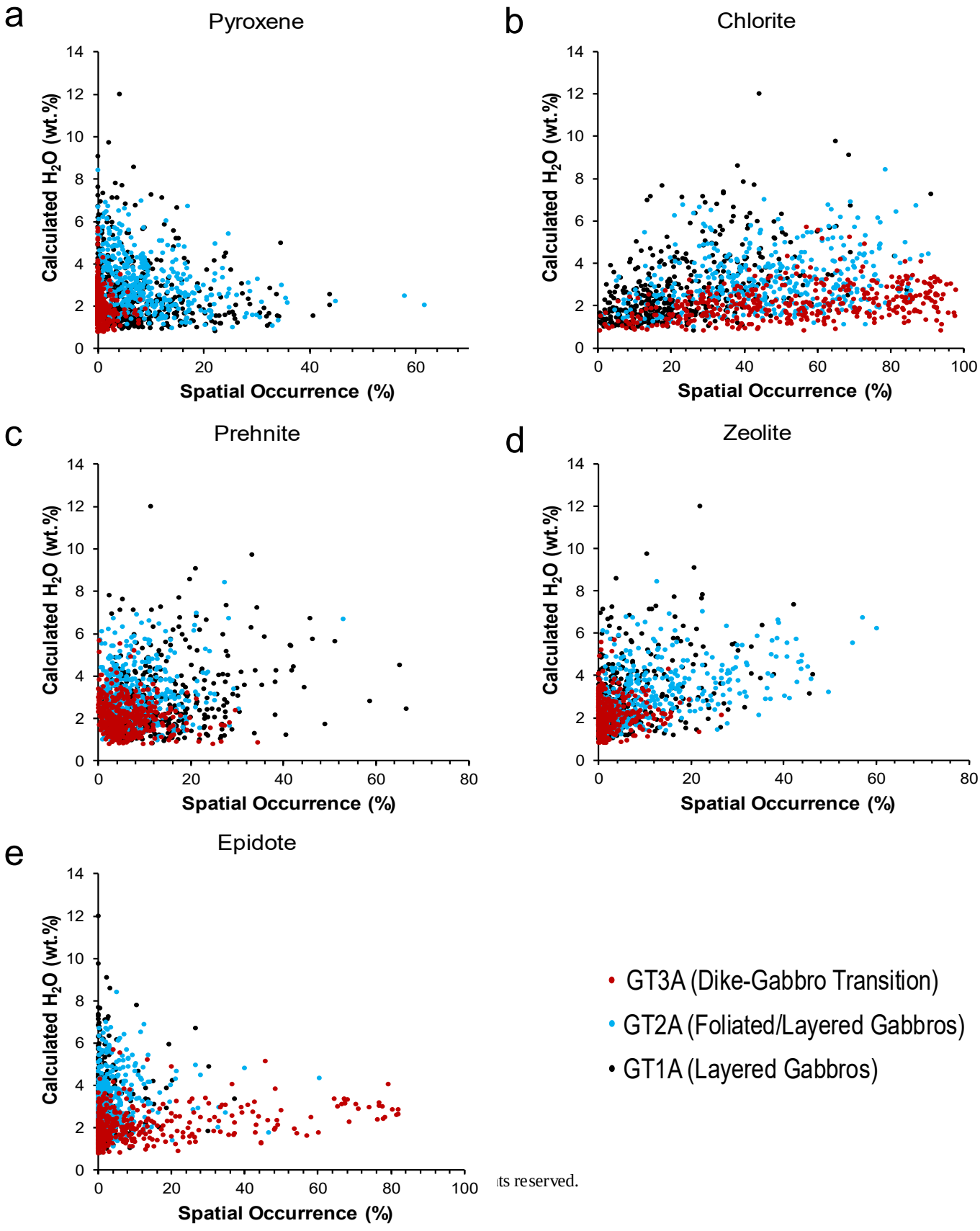
a
Pyroxene
Calculated H_2O (wt.%)
Spatial Occurrence (%)
b
Chlorite
Calculated H_2O (wt.%)
Spatial Occurrence (%)
c
Prehnite
Calculated H_2O (wt.%)
Spatial Occurrence (%)
d
Zeolite
Calculated H_2O (wt.%)
Spatial Occurrence (%)
e
Epidote
Calculated H_2O (wt.%)
Spatial Occurrence (%)
GT3A (Dike-Gabbro Transition)
GT2A (Foliated/Layered Gabbros)
GT1A (Layered Gabbros)